Theory-Enabled High-Throughput Screening of Ion Dissociation Explains Conductivity Enhancements in Diluted Ionic Liquid Mixtures

Rohit Chauhan[1], Rohan Sartape[1], Amey Thorat[2], Jindal K. Shah[2], and Meenesh R. Singh[1,*]

[1]Department of Chemical Engineering, University of Illinois at Chicago, Chicago, IL 60607, United States
[2]School of Chemical Engineering, Oklahoma State University, Stillwater, OK 74078, United States

Submitted to ACS Sustainable Chemistry & Engineering special issue on *"Emerging Investigators' Research and Opinions on Sustainable Chemistry and Engineering".*

Corresponding Author:
Prof. Meenesh R. Singh
Department of Chemical Engineering
929 W. Taylor St.
University of Illinois at Chicago
Chicago, IL 60607
Email: mrsingh@uic.edu
Tel: (312) 413-7673

Abstract

The growing demand for room-temperature ionic liquids (RTILs) for energy applications necessitates the development of an efficient screening platform. In this study, we have successfully developed a fully automated high-throughput RTIL screening platform specifically designed for assessing ionic conductivity. By utilizing the 96-wells of a microtiter plate as individual electrolysis cells, we measured ionic conductivity of 22 different RTILs, encompassing various combinations of cations and anions, and benchmarked the values with existing literature. We also employed the screening platform to investigate the conductivities of RTIL mixtures with a non-aqueous solvent, ethylene glycol (EG). Our results reveal specific combinations of RTILs with EG that result in approximately 200% enhancement in the conductivity values as compared to the pure RTILs. To understand the underlying mechanisms responsible for this enhancement, we developed a theoretical framework that considers factors such as degree of dissociation, viscous forces, and molal volume of the RTIL-EG mixtures. The optimized electrolyte mixture was then employed in the migration-assisted moisture gradient (MAMG) CO_2 capture process to study the effects of improved ionic conductivity on the energy efficiency of the process. Notably, the enhanced conductivity of the RTIL-EG mixture led to nearly 50% reduction in energy consumption for capturing CO_2. These outcomes highlight the effectiveness of our strategy in screening RTILs and improving existing processes. Moreover, our fully automated high-throughput setup, combined with the developed theoretical framework, provides a comprehensive platform for screening and studying RTIL mixtures with different solvents, enabling their application in various fields.

Keywords: Room Temperature Ionic Liquids (RTILs); High-throughput screening; Ion dissociation; Ionic Conductivity; Carbon Capture; Ion Mobility

1. Introduction

Room temperature ionic liquids (RTILs) are salts that are liquid at ambient temperatures with beneficial properties like nonflammability, low vapor pressure, and high ionic conductivity.[1] Some ionic liquids also exhibit significant improvement in properties such as ionic conductivity when diluted with other solvents, which makes them promising candidates to be used as electrolytes in various applications.[2] This non-monotonous behavior has often been attributed to the extent of ionic dissociation in such electrolytes, and several theories have been proposed to explain it. Further, the effects of ion dissociation are also known to impact the density,[3] viscosity,[4] surface tension,[5] vapor pressure,[6] chemical reactivity,[7, 8] and solubility of such mixtures.[9] Thus, understanding ion dissociation and developing a theoretical framework that can explain the behavior of such electrolytic mixtures of ionic liquids and molecular solvents is crucial to leverage such systems in various applications.

The IL/solvent systems are of specific interest to energy storage and conversion systems, where ionic conductivity dictates ohmic losses and concentration polarization. The contribution of ion mobility and dissociation towards the ionic conductivity of the solution is non-linear and challenging to deconvolute. The available ion dissociation studies cover only highly concentrated or very dilute systems. Ions accumulate into clusters at high concentrations of RTILs,[10, 11] which result in partial ionization.[12-14] Whereas, at very dilute concentrations of IL in solvent systems (<1 mM), complete dissociation can be expected as the solvent screens the attractive forces between the anion and cation,[15, 16] but there are exceptions.[1, 2] However, at an intermediate concentration range, the RTILs may undergo partial dissociation, the extent of which depends on the concentration of the RTIL and the type of solvent.[2, 17] The electrolyte morphology is especially sensitive to solvent concentration, and small changes in dilution often translate to more pronounced changes in the degree of dissociation. Consequently, the intensity of partial dissociation significantly influences the properties of the IL/solvent mixtures. Since there are limited approaches to understand the partial dissociation of ions, we probe into IL/ solvent electrolyte systems through the lens of degree of dissociation over comprehensive range of concentrations and try to correlate ionic conductivity with mixture composition.

Several computational studies involving molecular simulations, density functional theory (DFT) calculations, and machine learning techniques have been utilized to study the ionic conductivity of the ILs in different solvents.[18, 19] While these methods can be computationally intensive, the classical theory of ion dissociation can provide reasonably accurate estimations for IL/solvent mixtures with much lower computing power. For example, Li et al.[20] correlated the thermodynamic properties such as densities and osmotic coefficients of aqueous solutions by using the equation of state where the association energies of anions and cations are the fitted parameters. Some of these classical theories can explain the dissociation behavior of electrolytes;[21-24] however, these cannot be extended to describe the dissociation behavior and ionic conductivity of the RTILs for a full range of solvent concentrations. In recent years, ion dissociation of RTILs has been estimated by independently measuring the ionic conductivity and diffusion coefficients.[2] Watanabe's research group used electrochemical impedance spectroscopy (EIS) and pulse field gradient spin-echo nuclear magnetic resonance (PG-NMR) to measure ionic conductivity and diffusivity, respectively, of neat ionic liquids. Diffusivity was measured to calculate the ionic conductivity with the help of the Nernst-Einstein relationship. They estimated ionicity from the ratio of ionic molar

conductivity measured by EIS to that calculated from the Nernst-Einstein conductivity based on the ion-diffusion coefficient measured using PG-NMR. They reported that free ion fraction is directly correlated with ionicity,[25, 13] whereas, Lopes et al.[26] estimated the ILs ionicity in binary mixtures with the help of solubility data.

Both ionicity and diffusivity determine the ionic conductivity of solutions. Viscosity is known to affect the diffusivity and hence mobility of ions. Previous research on RTIL and solvent system used low-viscosity solvents to mix ILs, making it challenging to analyze the hydrogen bonding on the transport behavior due to the high viscosity of the IL.[27-32] However, recent studies have examined IL mixtures with slightly more viscous molecular solvents (e.g., ethylene glycol (EG) with a viscosity of 16.8 cP) to understand hydrogen bonding effects better. Studies are available for a mixture of ILs and EG report viscosity and density. The study of viscosity and density of 1-butyl-3-methylimidazolium tetrafluoroborate [BMIM][BF_4] and 1-ethyl-3-methylimidazolium tetrafluoroborate [EMIM][BF_4] in EG was performed,[33, 34] and negative deviation in viscosity measurement was observed in both the studies. Pal et al.[35] studied the behavior of mixing of aprotic and protic ILs in EG with the help of Fourier transform infrared spectroscopy (FT-IR). They observed that the interaction of hydrogen bonding was not imitated at the molecular level in the macroscopic behavior of the mixing. The hydrogen bonding and ion dissociation in a mixture of [BMIM][BF4] and EG was studied with the estimation of the viscosity of the solution, and it was observed that dilute ionic liquid solutions show isolated ion pairs surrounded by solvent. Cation-anion pair size increases non-linearly with concentration, leaving isolated solvent monomers in concentrated IL solutions.[36] However, studies for the conductivity analysis of the mixture of ILs and EG are very scarce. Recently, Nordness et al.[17] reported the conductivity measurement of the mixture of 1-ethyl-3-methylimidazolium trifluoroacetate [EMIM][TFA], 1-ethyl-3-methylimidazolium trifluoroacetate ethyl sulfate [EMIM][ESO_4], and 1-ethyl-3-methylimidazolium trifluoroacetate triflate [EMIM][OTF] in EG. The conductivities of all three mixtures attained a maximum at a particular composition and then decreased. They reported that this phenomenon was responsible due to the competition between free-ion concentration and viscous forces hindering ion diffusion.[17] The available studies only qualitatively highlight the ion dissociation phenomena for the limited number of IL/solvent systems. There is still a need for a comprehensive theory that enables a better understanding of how ion dissociation varies with the size/type of anions and cations, as well as their concentrations in a range of solvents.

The lack of a theoretical framework that can accurately predict the non-monotonous variation of ionic conductivity of electrolyte mixtures demands an intensive experimental campaign. Screening an extremely large number of electrolytes that can be formed from pure ionic liquids, their mixtures, and combinations with other solvents at different mixing ratios poses several logistical challenges, thereby making the process inefficient, slow, material and labor intensive. High-throughput screening is an approach that has been extensively used in the Pharmaceutical and Biotech industries for drug discoveries.[37] Based on the same strategy, screening of various solar catalysts,[38-41] and sensing proteins[42] have already been reported. However, literature on screening ionic liquids is scarce. Herein, we report a strategy to effectively screen binary IL with solvent mixtures to examine ion pair dissociation using conductivity.

The primary objective of high-throughput screening is to obtain the necessary ionic conductivity dataset to estimate ion dissociation and develop correlations. Such correlations will help prepare optimal compositions of IL mixtures to enhance ionic conductivity and hence reduce energy losses in several applications, including wastewater remediation,[43, 44] batteries,[45, 46] and biocatalysis.[47] Additionally, ILs have attained significant interest and have been identified as potential candidates amongst emerging technologies for carbon capture utilization and storage (CCUS). Application of IL in CCUS is an example studied, where we identify and implement an optimal composition of IL mixtures in CO_2 capture solvent (EG + KOH) to demonstrate percentage reduction in energy consumption for CO_2 capture and release via migration assisted moisture gradient (MAMG) process.

In this work, we developed an automated high-throughput platform to screen the conductivity of neat RTILs (details provided in Table S1 of the Supporting Information) and the mixture of RTILs and EG. For this purpose, we designed an electrode holder cell set for a robotic hand whose maneuvering was controlled by custom-built software for measuring the solution resistance. The measured resistance was then used to calculate the conductivity of that solution. A novel theoretical framework that relates ion dissociation with measured conductivity and concentration-dependent ion mobility has also been developed. The variation of ion dissociation with cation and anion type and their concentrations shed light on the mechanism of conductivity in the mixture of RTILs and EG. Finally, the migration-assisted moisture gradient (MAMG) process for carbon capture was tested as a potential application of enhanced conductivity in an ionic liquid and EG mixture.

2. Background and Theory

2.1. Theory of concentration-dependent ion dissociation and mobility

A simple theoretical framework is presented to evaluate the conductivity of neat RTIL and RTIL/solvent systems based on the estimation of the ion mobility which is comprised of ion dissociation. The basic equation of the conductivity of the solution is as follows:[48]

$$\sigma = F^2 \sum_i z_i^2 u_i c_i \tag{1}$$

where σ is conductivity (s/m), F is Faraday's constant (96,485 C/mol), u_i is the mobility of species (m^2.mol/J.s), c_i is the concentration of species (mol/m^3), z_i is charge of species. The neat RTIL and RTIL/solvent systems have two species, i.e., cation and anion; therefore, the conductivity of the RTILs system could be expressed as follows from eq. (1):

$$\sigma = F^2 z_+^2 u_+ c_+ + F^2 z_-^2 u_- c_- \tag{2}$$

where u_+ and u_- are the mobility of the cation and anion, respectively; c_+ and c_- are the concentration of cation and anion, respectively; and z_+ and z_- are the charges of cation and anion, respectively. Since the concentration of the cation and anion is the same in the solution, then $c_+ = c_- = c_{+/-}$ and $z_+ = z_- = z$, therefore eq. (2) could be expressed as follows:

$$\Rightarrow \sigma = F^2 z^2 c_{+/-} (u_+ + u_-) \tag{3}$$

$$\Rightarrow \sigma = F^2 z^2 c_{+/-} u_+ \left(1 + \frac{u_-}{u_+}\right) \tag{4}$$

The Nernst-Einstein equation relates the ionic mobility with the diffusion:[48, 49]

$$D_i = RTu_i \tag{5}$$

$$\Rightarrow u_i = \frac{D_i}{RT} \tag{6}$$

$$\Rightarrow \frac{D_-}{D_+} = \frac{u_-}{u_+} \tag{7}$$

where D_i is the diffusion coefficient of species i (m^2/s), R is the universal gas constant (J/mol.K), and T is the temperature (K).

Instead of direct measurement of ion diffusivity, it could be estimated from other properties. There are different models with complex ranges that have been developed to explain ion transport. However, despite its simplicity, the Wilke and Chang equation is a good approximation of ion diffusivity. Therefore, the diffusivity of ionic species is defined as:[50]

$$D_i = \frac{(117.3\times10^{-18})(\phi M_S)^{0.5}T}{\eta \upsilon_i^{0.6}} \tag{8}$$

where D_i is the diffusivity of species i (m^2/s), M_S is the Molecular weight of solvent (kg/kmol), T is the temperature (K), η is viscosity (kg/m.s) of a solution, υ_i is species molal volume at normal boiling point (m^3/kmol), φ is Association factor for solvent (φ=1 for ethylene glycol). The molal volume of the ions was estimated by Schotte's methodology.[51] For cation and anion of the ionic liquid, diffusivity could be expressed as follows:

$$D_+ = \frac{(117.3\times10^{-18})(\phi M_S)^{0.5}T}{\eta \upsilon_+^{0.6}} \tag{9}$$

$$D_- = \frac{(117.3\times10^{-18})(\phi M_S)^{0.5}T}{\eta \upsilon_-^{0.6}} \tag{10}$$

$$\Rightarrow \frac{D_-}{D_+} = \left(\frac{\upsilon_+}{\upsilon_-}\right)^{0.6} \tag{11}$$

By combining eq. (7) and (11):

$$\Rightarrow \frac{u_-}{u_+} = \left(\frac{\upsilon_+}{\upsilon_-}\right)^{0.6} \tag{12}$$

Now, combining eq. (4) with eq. (13) and after rearrangement:

$$\sigma = F^2 z^2 c_{+/-} u_+ \left(1 + \left(\frac{\upsilon_+}{\upsilon_-}\right)^{0.6}\right) \tag{13}$$

RTILs have free ions that are responsible for the conductivity of the RTILs, and ion dissociation (ξ) is the ratio of the concentration of the free ions (cation/anion) and concentration of the ionic liquid, and it could be expressed as follows:

$$\xi = \frac{c_{+/-}}{c_{IL}} \tag{14}$$

Now, combining eq. (13) and (14):

$$\sigma = F^2 z^2 \xi c_{IL} u_+ \left(1 + \left(\frac{\upsilon_+}{\upsilon_-}\right)^{0.6}\right) \tag{15}$$

$$\Rightarrow \xi u_+ = \frac{\sigma}{F^2 z^2 c_{IL}\left(1+\left(\frac{\upsilon_+}{\upsilon_-}\right)^{0.6}\right)} \tag{16}$$

For infinite dilute solution ($x_{\text{solvent}} \rightarrow 1$), the product of ion dissociation and mobility is given by,

$$\lim_{x_{solvent}\to 1} \xi u_+ = \xi_\infty u_{+,\infty} \tag{17}$$

where $u_{+,\infty}$ is the mobility of the cation at infinite dilution and ξ_∞ is the ion dissociation at infinite dilution. Their product can be estimated from experimental molar conductivity by taking infinite dilution limits on eq. (16) as follows:

$$\xi_\infty u_{+,\infty} = \lim_{x_{solvent}\to 1} \frac{\sigma}{F^2 z^2 c_{IL}\left(1+\left(\frac{\upsilon_+}{\upsilon_-}\right)^{0.6}\right)} = \frac{1}{F^2 z^2\left(1+\left(\frac{\upsilon_+}{\upsilon_-}\right)^{0.6}\right)} \lim_{x_{solvent}\to 1} \frac{\sigma}{c_{IL}} \tag{18}$$

Since it is difficult to measure ion dissociation at infinite dilution, we can estimate the relative ion dissociation defined as $\xi_r = \xi / \xi_\infty = c_{+/-} / c_{+/-,\infty}$ at different concentrations of ionic liquids. For this purpose, we re-write product of ion dissociation and mobility in terms of relative quantities as follows:

$$\xi u_+ = \xi_r \xi_\infty u_{+,r} u_{+,\infty} = \left(\xi_r u_{+,r}\right)\left(\xi_\infty u_{+,\infty}\right) \tag{19}$$

The relative mobility is related to the viscosity of the solution and radius of the solvated cation, as follows:

$$u_{+,r} = \frac{u_+}{u_{+,\infty}} = \frac{\eta_\infty}{\eta}\frac{r_{+,\infty}}{r_+} \tag{20}$$

The viscosity η of a solution can be determined from the mixing rule of the ideal solution, which is as follows:[17]

$$\log\eta = x_{IL}\log\eta_0 + \left(1-x_{IL}\right)\log\eta_\infty \tag{21}$$

where η_∞ is the viscosity of the solvent, η_0 is the viscosity of the pure ionic liquid, and x_{IL} is the mole fraction of ionic liquid in binary solution.

Rearranging the above equation gives,

$$\frac{\eta_\infty}{\eta} = \left(\frac{\eta_\infty}{\eta_0}\right)^{x_{IL}} \tag{22}$$

Combining eq. (19), eq. (20) and eq. (22),

$$\Rightarrow \xi u_+ = \xi_r \xi_\infty u_{+,r} u_{+,\infty} = \left(\xi_r u_{+,r}\right)\left(\xi_\infty u_{+,\infty}\right) = \xi_r \left(\frac{\eta_\infty}{\eta_0}\right)^{x_{IL}} \frac{r_{+,\infty}}{r_+}\left(\xi_\infty u_{+,\infty}\right) \tag{23}$$

The solvation number for larger cations in non-aqueous solutions is typically lower than the solvation number in aqueous solutions.[52] This is due to the lower polarity of non-aqueous solutions. In such cases, we can assume a monolayer of primary solvation shell of thickness approximately the diameter of the solvent molecule, which varies linearly with the mole fraction of the solvent.

$$r_+ = r_{+,0} + x_s\ \Delta r_{+,\infty} = r_{+,0} + \left(1 - x_{IL}\right)\Delta r_{+,\infty} \tag{24}$$

where $r_{+,0}$ is the van der Waal radius of the cation in neat IL solution, $\Delta r_{+,\infty}$ is the solvation shell thickness of the cation at infinite dilution, and x_s is the mole fraction of the solvent. Rearranging the above equation,

$$\frac{r_{+,\infty}}{r_+} = \frac{r_{+,0} + \Delta r_{+,\infty}}{r_{+,0} + \left(1 - x_{IL}\right)\Delta r_{+,\infty}} = \frac{1}{1 - x_{IL}\left(\dfrac{\Delta r_{+,\infty}}{r_{+,\infty}}\right)} \tag{25}$$

Since $\Delta r_{+,\infty} = 2r_s$ (diameter of solvent) and $r_{+,0} = r_{+,IL}$, the above expression reduces to

$$\frac{r_{+,\infty}}{r_+} = \frac{1}{1 - x_{IL}\left(\dfrac{2r_s}{r_{+,IL} + 2r_s}\right)} \tag{26}$$

Now, substituting the relative cation radius and relative viscosity back into the expression for relative migration yields

$$u_{+,r} = \frac{\eta_\infty}{\eta}\frac{r_{+,\infty}}{r_+} = \left(\frac{\eta_\infty}{\eta_0}\right)^{x_{IL}} \frac{1}{1 - x_{IL}\left(\dfrac{2r_s}{r_{+,IL} + 2r_s}\right)} \tag{27}$$

Now, substituting eq. (27) into eq. (19) and equating with eq. (16) will yield the expression for relative ion dissociation constant-

$$\xi_r = \frac{\sigma}{F^2 z^2 \left(\xi_\infty u_{+,\infty}\right) c_{IL}\left(1 + \left(\dfrac{\upsilon_+}{\upsilon_-}\right)^{0.6}\right)} \left(\frac{\eta_0}{\eta_\infty}\right)^{x_{IL}} \left(1 - x_{IL}\left(\frac{2r_s}{r_{+,IL} + 2r_s}\right)\right) \tag{28}$$

This equation can be further simplified by defining ionic conductivity at infinite dilution $\left(\sigma_\infty\right)$ and relative mobility (eq. 20)

$$\xi_r = \frac{\sigma}{\sigma_\infty}\frac{u_{+,\infty}}{u_+} = \frac{\sigma_r}{u_{+,r}} \tag{29}$$

Using such formulation, we can estimate the ion dissociation of neat RTIL and RTIL/solvent mixture. One can observe the significance of the eq. (29) that the present methodology of ion mobility comprised of ion dissociation requires concentration of ionic liquid (c_{IL}), ionic conductivity (σ) measured by EIS and molal volume of ions at normal boiling point (υ) calculated by Schotte's method. In addition, a relation between ion dissociation and equilibrium constant through thermodynamic chemistry is given in section S1 (Supporting Information). It further relates the activity coefficient of the ions with ion dissociation.

2.2. Chemistry of CO_2 capture and release by migration-assisted moisture gradient (MAMG)

MAMG is based on a humidity swing process under an external bias that can achieve high CO_2 capture flux from dilute sources.[53-55] Fundamentally, a humidity swing approach, proposed by Lackner and coworkers,[56, 57] utilizes a quaternary amine-based ion exchange resin supported on a membrane that creates a water concentration gradient by separating dry and wet compartments. The membrane can absorb CO_2 in the form of HCO_3^- ions and release CO_2 in

the wet compartment. Similarly, the MAMG process continuously absorbs CO_2 in an organic liquid (dry compartment) to form HCO_3^- ions (Eq. (30)) and then under an influence of an external electric field, these ions migrate to an aqueous compartment to decompose and yield CO_2, water and CO_3^{2-} ions. Extensive details on the CO_2 capture kinetics, effect of CO_2 partial pressure and membrane thickness have been discussed in our previous works.[54]

$$CO_2 + OH^- \rightleftharpoons HCO_3^- \quad (30)$$

$$2HCO_3^- \rightleftharpoons CO_2 + H_2O + CO_3^{2-} \quad (31)$$

3. Experimental Methods

3.1. Materials

Room temperature ionic liquids (RTILs) used in the study were obtained from IoLiTec and were used without further purification. All RTILs structures, abbreviation, and purity information is shown in Table S1 (supporting information). The ethylene glycol of 99% purity and silver wire of 99% purity was obtained from Sigma Aldrich. It might be important to list the number of ionic liquids to impress upon the amount of work accomplished.

3.2. Automated mixture preparation of RTILs and EG

Prior to the use in an experiment, RTILs, and ethylene glycol were subjected to drying at 60℃ in a vacuum oven for 12 hrs. The water content of ILs and EG was determined by Metrohm Karl Fisher Titrator (EcoKF Titrator). It was ensured that the water content was less than 0.1% before the experiment. DragonFly liquid handling system was used to create binary mixtures of RTIL and EG in each well across the microtiter plate. After the liquid dispensing step, the 96-well plate was placed in a vibrator (MTI Corporation Ltd.) for 15 min with an evaporation shield to minimize contact with the air. A schematic illustration of the automated mixing of RTIL and EG is shown in Figure 1.

3.3. Automated high-throughput conductivity measurement

A custom electrode holder cell for conductivity measurement was 3D printed, shown in Figure 1, which housed two silver electrodes (500 μm diameter). Each well of the 96-well plate acts as an electrolyte cell, and the cell constant (1.1943/cm) was obtained by calibrating against the aqueous solution of KCl of 0.01 M, 0.1 M, 0.5 M, and 1 M concentration by standard procedure.[12, 58] Dobot Magician was used as a robotic hand to maneuver and place two electrodes in each microtiter plate well for conductometric study. Ionic conductivity measurements were carried out by performing Electrochemical Impedance Spectroscopy (EIS) on Biologic SP-300 potentiostat. The interfacing between the motion of the robotic hand and EIS measurement was enabled through SweepMe! software (www.sweepme.net). Therefore, the ionic conductivity of all neat RTILs was measured by measuring RTILs solution's resistance in a fully automated system comprised of a liquid dispenser unit, a 96-well plate, and a robotic hand synchronized with SweepMe! Software. The SweepMe! Software consists of the control of robotic hand movement as well as EIS measurement of the solution. Therefore, this software was developed to measure the resistance of the solution in each well of the 96-well plate with a robotic hand (with an electrode holder) moving towards each well. The cross-contamination of the electrode surface as the robotic arm moves electrodes from one cell to another was avoided by filling the cells of the alternate column of the 96-well plate with isopropyl alcohol to wash the electrode before measurements. All EIS measurements were

obtained at 298.15K and performed on each binary mixture with a 20mV sinusoidal pulse in the 100 kHz to 30 Hz frequency range. All the conductivity values are presented with a standard deviation of triplet measurements. A schematic illustration of the automated high-throughput conductivity measurement is shown in Figure 1.

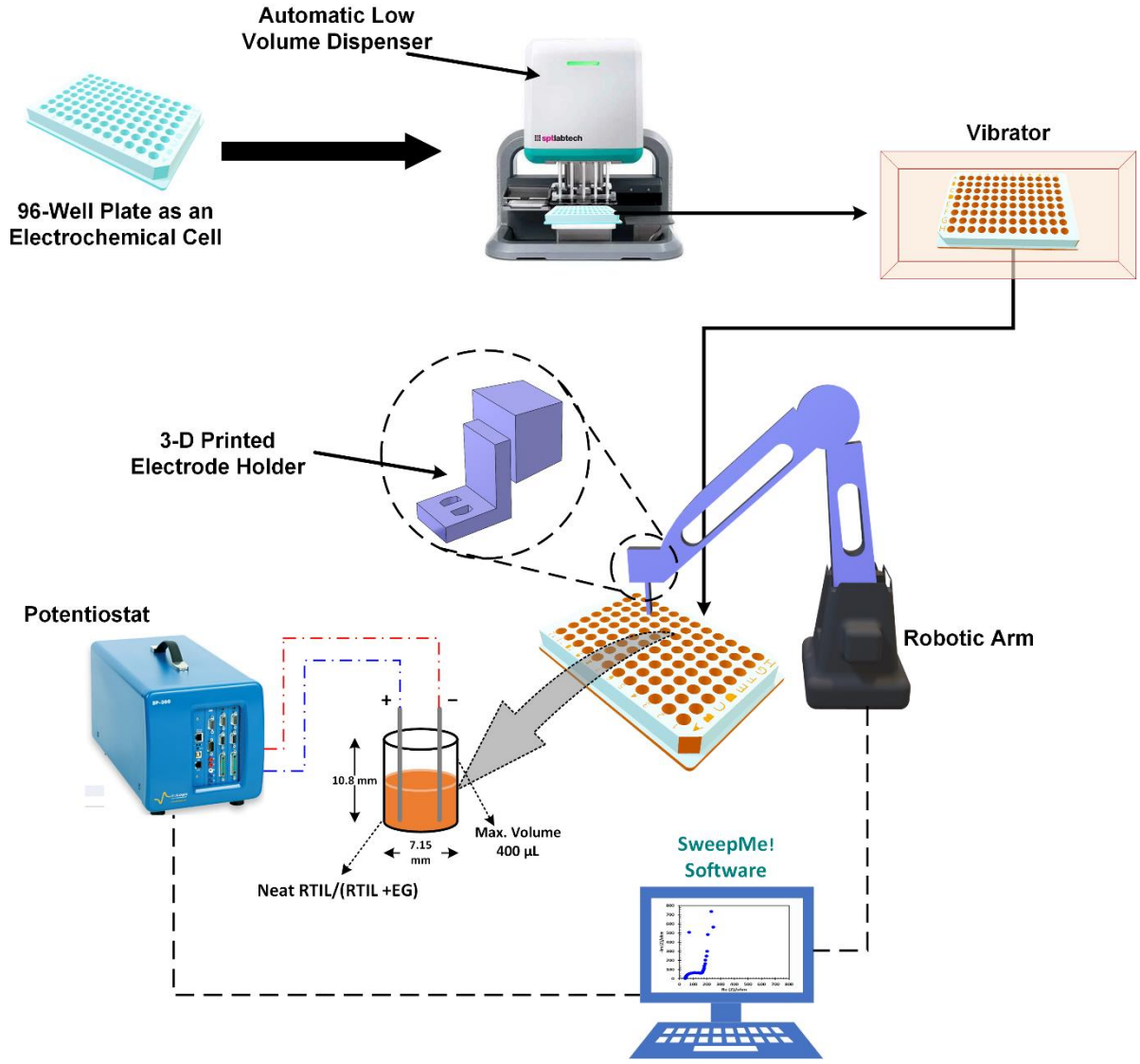

Fig. 1. Schematic illustration of the automation system for high-throughput screening of conductivity of neat RTILs and the mixture of RTILs and EG.

3.4. Migration-assisted moisture gradient (MAMG) experiment

The experiments were carried out in a custom 3D-printed cell which consists of an aqueous compartment containing 0.1M KOH pre-equilibrated with CO_2 (pH=7.8) and an organic liquid compartment containing a mixture of 1.2M of KOH in EG. For the MAMG experiment with the mixture of IL with EG, the organic liquid was prepared additionally with the relevant IL mol fraction (at which the maximum ionic conductivity was observed). Solutions in both compartments were continuously recirculated with a Cole Parmer MasterFlex multi-drive peristaltic pump. An anion exchange membrane from SnowPure (Excellion A200, pretreated with water at 80^{o}C) was sandwiched to separate the aqueous and organic

compartments. Migration in the MAMG process was enabled by using Cu mesh (4cm^2, American Elements 99.99% pure) as cathode and using Carbon Toray paper (4cm^2, Fuel Cell Store, 190um Toray 060) as anode placed in organic and aqueous compartments. A DC source from Eventek at constant current mode facilitated the migration of ions from the organic side to the aqueous side. During the MAMG experiment, a simulated flue gas of 90% N_2 and 10% CO_2 was continuously bubbled in the organic liquid. The migration flux of the dissolved CO_2 was continuously monitored as a function of the pH decrease in the aqueous side by a Thermo Orion A111 pH probe. A schematic diagram of the electrochemical setup for MAMG process is available in our already-published article.[54]

4. Results and Discussion

4.1. Comparison of ionic conductivity measured via high-throughput approach and previously reported ionic conductivity of neat RTILs

All the calculated conductivity obtained from the fully automated high-throughput system (mentioned in the Experimental Methods section) with previously reported conductivity values with conventional methods is shown in Figure 2. The previously available conductivity data of the neat RTILs have been referenced from the IL Thermo[28, 59-77] and IoLiTec. We have used different RTIL systems with different cation and anion combinations, shown in Table S1 (supporting information). The list contains different imidazolium cations ($[EMIM]^+$, $[BMIM]^+$, $[HMIM]^+$, and $[OMIM]^+$), and pyridinium cation ($[BPM]^+$, $[B3MPY]^+$, and $[4MBBP]^+$) with tetrafluoroborate anion ($[BF_4]^-$); different imidazolium cation ($[EMIM]^+$, $[BMIM]^+$, and $[OMIM]^+$), and one pyrrolidinium cation ($[BMPYRR]^+$) with trifluoromethanesulfonate/triflate anion ($[OTF]^-$); $[EMIM]^+$ and $[BMPYRR]^+$ cation with dicyanamide $[DCA]^-$ anion; [MPI]+, $[BMIM]^+$, and $[HMIM]^+$ cation with iodide $[I]^-$ anion; $[EMIM]^+$ with ethyl sulfate $[ESO_4]$ anion, hydrogen sulfate $[HSO_4]^-$ anion, thiocyanate $[SCN]^-$ anion, diethyl phosphate $[DEP]^-$ anion; $[MMIM]^+$ with methyl phosphate $[DMP]^-$ anion; and ethyl ammonium with nitrate anion [EAN]. It can be seen from Figure 2 that the fully automated high-throughput setup measured the conductivity, which matches well with the previously reported values. Table 1 illustrates the cation-anion combinations for which ionic conductivity was obtained, and Table S2 (supporting information) shows the average conductivity values of three experiments of all the RTILs.

Table 1. Different combinations of cations and anions of RTILs studied in this work.

Anion→	$[BF4]^-$	$[OTF]^-$	$[DCA]^-$	$[ESO_4]^-$	$[I]^-$	$[SCN]^-$	$[DEP]^-$	$[N]^-$	$[DMP]^-$	$[HSO_4]^-$
Cation↓										
$[EMIM]^+$	✓	✓	✓	✓		✓	✓			✓
$[BMIM]^+$	✓	✓			✓					
$[HMIM]^+$	✓				✓					
$[OMIM]^+$	✓	✓								
$[BPM]^+$	✓									
$[B3MPY]^+$	✓									
$[4MBBP]^+$	✓									
$[MPI]^+$					✓					
$[BMPYRR]^+$		✓	✓							
$[MMIM]^+$									✓	
$[EA]^+$								✓		

The estimated conductivity values obtained from automated high-throughput setup for imidazolium-based cation and $[BF_4]^-$ anion, i.e., $[EMIM][BF_4]$, $[BMIM][BF_4]$, $[HMIM][BF_4]$, and $[OMIM][BF_4]$ was of 1.4±0.008 s/m, 0.352±0.004 s/m, 0.116±0.00011 s/m, and 0.069±0.0001 s/m, respectively (estimated conductivity are represented with a standard deviation of triplet experiments). These values agree with the previous reported, i.e., 1.563±0.06 s/m, 0.356±0.054 s/m, 0.118 s/m, and 0.067±0.007 s/m, respectively (Figure 2).[76, 78, 79] The agreement also demonstrates the high-throughput screening apparatus constructed in this study is capable of accurately providing ionic conductivity information over, at least, one order of magnitude. As the alkyl chain of the imidazolium-based tetrafluoroborate, RTIL, increases from C_2 to C_8, the conductivity of this RTIL system decreases. Therefore, this RTIL system has the following trend of ionic conductivity, $[EMIM][BF_4]$ > $[BMIM][BF_4]$ > $[HMIM][BF_4]$ > $[OMIM][BF_4]$. The reason for such a trend could be the high viscosity of RTIL, which increases with the increase of the alkyl group, i.e., from 0.0338 to 0.76 Pa.s, for $[EMIM][BF_4]$ to $[OMIM][BF_4]$, respectively. The viscosity of all neat RTILs was provided by the manufacturer (IoLiTec).

Rilo et al.[80] also reported that the conductivity decreases with the increase of the alky chain. In addition, it was demonstrated that with the increase of the alkyl chain length, the role of the electrostatic interaction decreases,[81] which was further verified by Nordness and Brennecke[2], and they also reported that longer alkyl chain length is responsible for the stronger van der Waals interaction resulted in the decrease in ion dissociation which corresponds the decrease in ionic conductivity. It could be observed that the conductivity of the neat [BPM][BF4] RTIL from Figure 2 was estimated by automated high-throughput setup; it has a maximum of 0.229±0.00007 s/m among pyridinium-based cation paired with $[BF_4]^-$ anion, i.e., $[B3MPY][BF_4]$, and $[4MBBP][BF_4]$ which have a conductivity of 0.171±0.00016 s/m, and 0.162±0.00002 s/m, respectively. These values are also in good agreement for $[BPM][BF_4]$, $[B3MPY][BF_4]$, and $[4MBBP][BF_4]$ with previous conductivity values of 0.210, and 0.185 s/m, respectively (Figure 2).

The next RTIL system consists of imidazolium, pyrrolidinium cation, and trifluoromethanesulfonate/triflate $[OTF]^-$ anion. The estimated conductivity obtained from the automated setup of neat [EMIM][OTF], [BMIM][OTF], and [OMIM][OTF] was 0.830±0.004 s/m, 0.251±0.005 s/m, and 0.065±0.0001 s/m, respectively. It follows a similar trend as imidazolium cation and $[BF4]^-$ anion-based RTILs; the conductivity of pyrrolidinium-based cation trifluoromethanesulfonate/triflate $[OTF]^-$ anion decreases with the increase of the alkyl chain length. The estimated conductivity for pyrrolidinium cation-based trifluoromethanesulfonate/triflate anion [BMPYRR][OTF] RTIL was 0.176±0.0001 s/m. These conductivities have good agreement with previous values of the conductivity of 0.907±0.035 s/m, 0.294±0.005 s/m, 0.058 s/m, and 0.185 s/m for [EMIM][OTF], [BMIM][OTF], [OMIM][OTF], and [BMPYRR][OTF], respectively.[63, 76] The next RTIL system consisting of $[EMIM]^+$ and $[BMPYRR]^+$ cation and $[DCA]^-$ anion was used for the estimation of conductivity with the help of an automated setup. The estimated conductivity for [EMIM][DCA] and [BMPYRR][DCA] was 2.817±0.005 s/m and 0.99±0.004 s/m and matches well with previously reported conductivity which was 2.83±0.116 s/m, and 1.19±0.02 s/m, respectively (Figure 2).[69, 82] The conductivity of $[I]^-$ anion with $[MPI]^+$, $[BMIM]^+$, and $[HMIM]^+$ cation RTIL system was obtained by automated setup, and estimated values were 0.112±0.0005 s/m, 0.064±0.0001 s/m, and 0.014±0.0002 s/m, respectively. It also follows a similar trend, i.e., with the increase of the alkyl chain of the RTIL, the conductivity of the respected RTIL decreases. It also has matching conductivity values of 0.096 s/m, 0.057 s/m, and 0.014 s/m with previous reported data for [MPI][I], [BMIM][I], and [HMIM][I], respectively (Figure 2).[61]

The other anionic groups with imidazolium-based cation and ethyl sulfate and hydrogen sulfate RTILs were also used to estimate their conductivity with an automated setup. The estimated conductivity was of 0.371±0.0001 s/m, and 0.050±0.0002 s/m whereas reported conductivity values was of 0.382±0.08 s/m, and 0.052 s/m for [EMIM][ESO_4], and [EMIM][HSO_4], respectively (Figure 2).[72] The automated estimation of the conductivity matches well with previously reported values. It can also be observed that the conductivity of [EMIM][ESO_4] is higher than [EMIM][HSO_4]. Since [EMIM][ESO_4] has a viscosity of 0.0942 Pa.s lower than the viscosity of [EMIM][HSO_4], which has a viscosity of 1.51 Pa.s, therefore viscous forces are a significant parameter to define the conductivity of neat RTIL. The estimated conductivity of the [MMIM][DMP] and [EMIM][DEP] was of 0.141±0.0001 s/m, and 0.079±0.0001 s/m whereas reported conductivity was of 0.084 s/m, and 0.090±0.0001 s/m, respectively (Figure 2).[70] Similarly, the estimated conductivity for [EMIM][SCN] and [EAN] was of 2.218±0.002 s/m, and 2.093±0.001 s/m, whereas reported conductivity was of 1.813±0.06 s/m, and 2.259±0.01 s/m, respectively (Figure 2).[60, 73]

Overall, the estimation of the conductivity of neat RTILs through the measurement of solution resistance with automation follows a good agreement with the previously available conductivity data of the respected RTIL. Therefore, this automated configuration represents a potentially unique approach for rapidly screening RTILs suited for applications where ionic conductivity is a key determining factor.

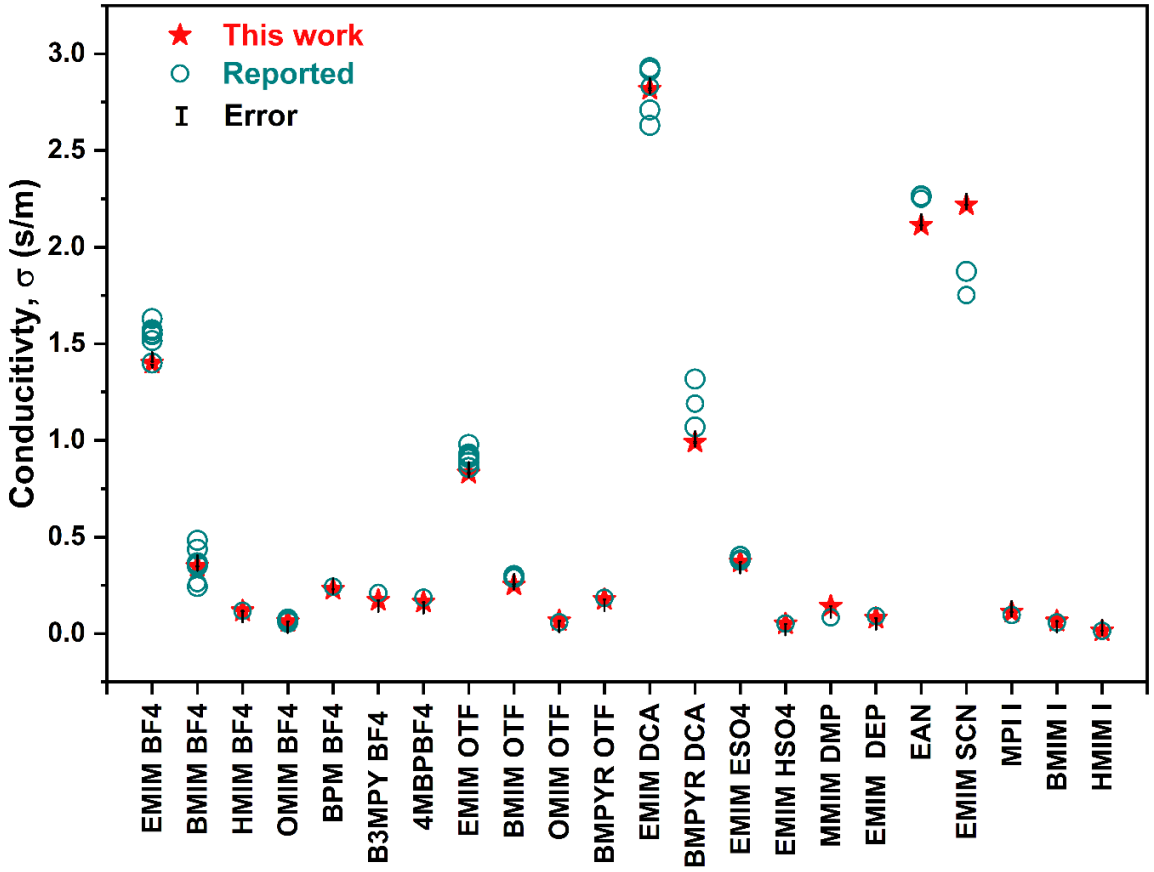

Fig. 2. Measured ionic conductivities of neat RTILs using the high-throughput setup that are benchmarked against previously reported data at 298 K (Data taken from IL Thermo and IoLiTec).

4.2. Ionic conductivity and ion mobility comprised of ion dissociation in RTIL and EG mixtures

The ionic conductivity of the mixture of RTILs and EG was estimated with the high-throughput setup discussed in the Experimental Methods section at 298.15 K. The relative ionic mobility comprised of ion dissociation is calculated with the help of Eq. (28) to compare its trend with ionic mobility. The ionic conductivity and relative ion dissociation (ξ_r) behavior of the RTIL system consisting of imidazolium cation ($[EMIM]^+$, $[BMIM]^+$, $[HMIM]^+$, and $[OMIM]^+$ with tetrafluoroborate anion ($[BF_4]^-$) in EG is shown in Figure 3(a), and 3(b), respectively. It could be observed that the conductivity increases with the increase of the ionic liquid mole fraction, reaching a maximum and then decreases approaching the conductivity of the neat RTIL. Also, as the alkyl chain length increases, the ionic conductivity behavior of the respective RTIL system decreases, similarly observed for neat RTILs conductivity. Therefore, this RTIL system has the following trend of ionic conductivity, $[EMIM][BF_4] > [BMIM][BF_4] > [HMIM][BF_4] > [OMIM][BF_4]$. A similar trend was also reported for the mixture of RTILs in aqueous and non-aqueous solvents (e.g., ethanol, EG, glycerol, triethanolamine).[12, 17, 80] All RTIL systems showed a maximum in the ionic conductivity at a given concentration of the RTIL in EG; however, the composition was different for the maximum conductivity value.

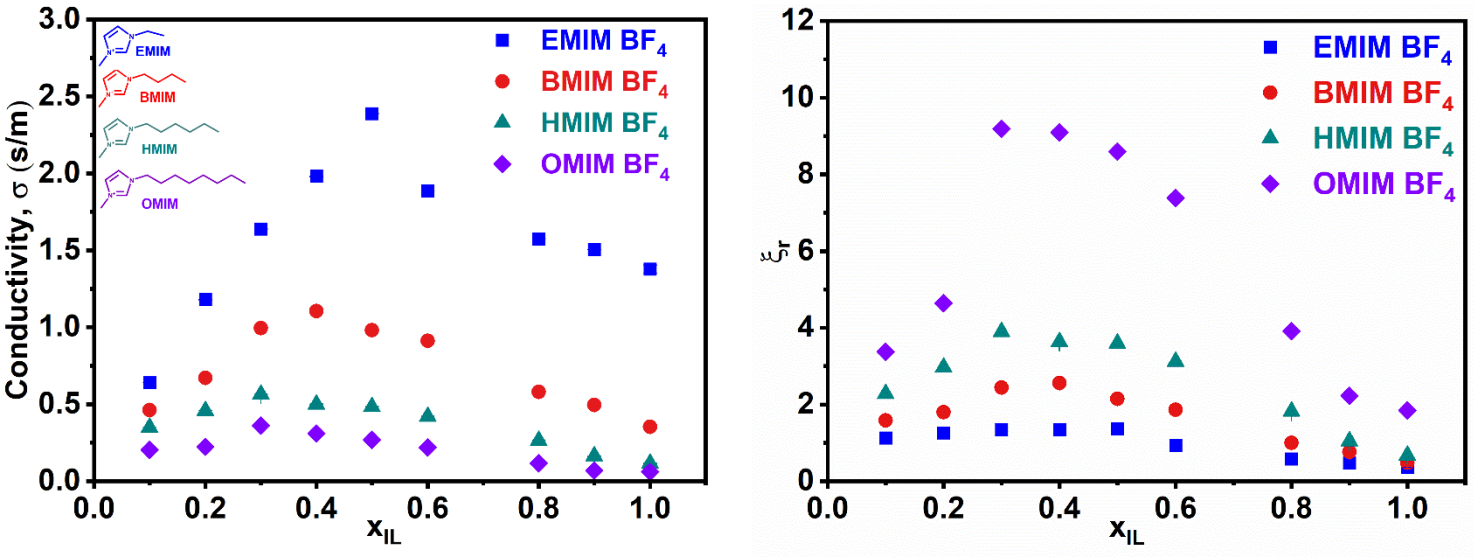

Fig. 3. (a) Ionic conductivity of [EMIM][BF_4], [BMIM][BF_4], [HMIM][BF_4], and [OMIM][BF_4] RTILs in EG at different mole fractions of ionic liquid estimated by the high-throughput system at 298.15 K; (b) relative ion dissociation of [EMIM][BF_4], [BMIM][BF_4], [HMIM][BF_4], and [OMIM][BF_4] RTILs in EG for IL mole fraction.

The maximum ionic conductivity (σ_{max}) with its composition for all the RTIL systems is shown in Figure 4. It could be observed from Figure 4 for [EMIM][BF_4], [BMIM][BF_4], [HMIM][BF_4], and [OMIM][BF_4] that as the alkyl chain length increases, the mole fraction of ionic liquid necessary to achieve the maximum decreases. The maximum conductivity is obtained at $x_{IL,max}$=0.5 for the lowest alkyl chain in this RTIL system, i.e., [EMIM][BF_4], whereas the maximum conductivity is obtained at a lower $x_{IL,max}$=0.4 for [BMIM][BF_4]. For [HMIM][BF_4] and [OMIM][BF_4], the maximum conductivity was obtained at $x_{IL,max}$=0.3. Rilo et al.[78] also observed similar behavior for $[EMIM]^+$, $[BMIM]^+$, $[HMIM]^+$, and $[OMIM]^+$ cationic group paired with $[BF_4]^-$ anion in ethanol at $x_{IL,max}$=0.54, 0.28, 0.18, and 0.18, respectively, at 298.15 K temperature. It could be observed in Rilo's study that the composition for $[HMIM]^+$ and $[OMIM]^+$ is same, which was also obtained for the present study. Interestingly, the ionic liquid mole fractions at which ionic conductivity maximum is observed are higher in ethylene glycol than those in ethanol except [EMIM][BF_4]. The behavior could be attributed to a higher dielectric constant for ethylene glycol, enabling a higher dissociation of ionic liquids due to greater screening of electrostatic interactions. Furthermore, the presence of two -OH groups in ethylene glycol as opposed to one in ethanol provides more opportunities for hydrogen bonding in ethylene glycol, resulting in improved solvation of charged species.

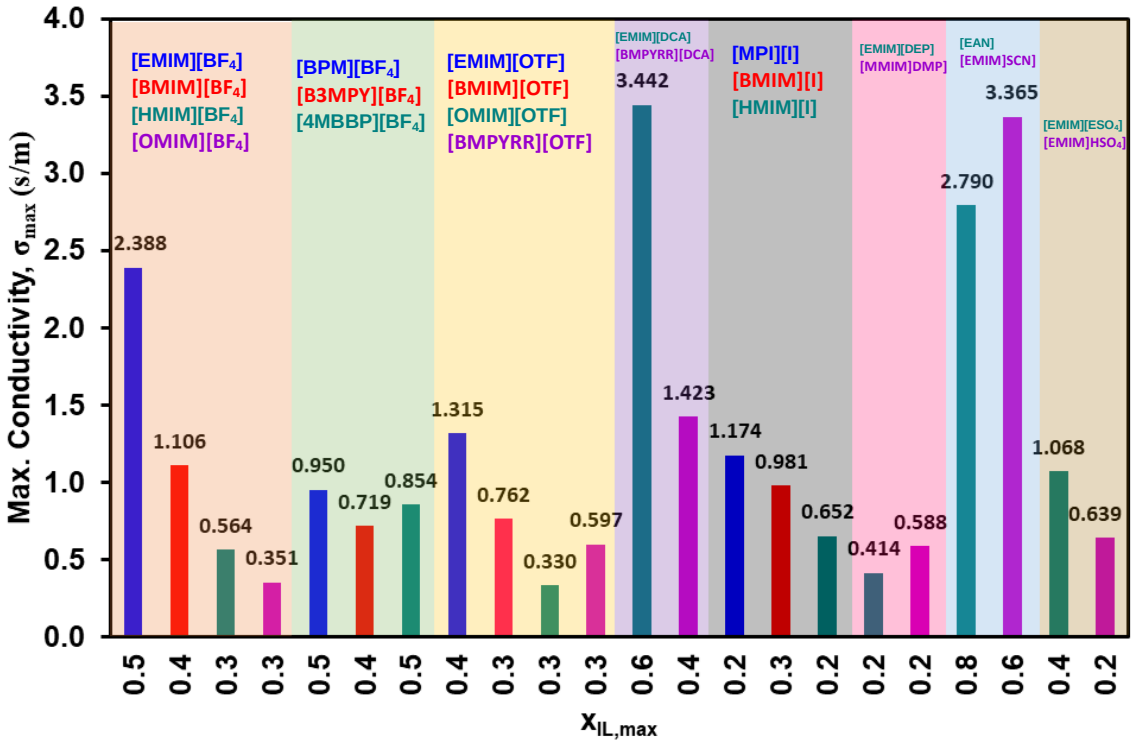

Fig. 4. Maximum conductivity of RTIL mixture in EG at the respective composition of the ionic liquid in EG. σ_{max} is the maximum conductivity of RTIL and $x_{IL,max}$ is the mole fraction at which maximum conductivity is obtained.

After comparing the behavior of ξ_r with the ionic conductivity, it could be observed that the ξ_r of this RTIL system showed a similar trend as ionic conductivity (Figure 3(b)). This potentially validates our hypothesis that the ion dissociation governs the observed trend of increasing conductivity with the composition of ionic liquid and reaching the maximum value at a particular composition, then approaching the ionic conductivity of neat RTIL. Therefore, ξ_r is a significant parameter for any RTIL system to define the dissociation of the ions in any molecular solvent. In addition, this phenomenon could also be identified as the competing effects of enhancing free ions concentration against the enhanced viscous forces hindering the diffusion of ions in the system. Therefore, viscous forces and free ions are the significant parameters that control the mobility of the ions and, thus, the ionic conductivity. It could also be observed from Eq. (1) that the ionic conductivity is defined by the ion mobility (u_i). For this purpose, the behavior of the solution viscosity (η) (calculated from Eq. (21)) and relative mobility of cations ($u_{+,r}$) (calculated from Eq. (27)) of all RTILs in EG with the composition of RTILs is shown in Figure S1 and Figure S2 (supporting information), respectively. It could be observed from Figure S1 (supporting information) that the viscosity of the solution of the RTIL and EG increases with the increase of the RTIL concentration from infinite dilution condition, i.e., the viscosity of the solvent, EG, to the neat RTIL viscosity. Figure S2(a) (supporting information) shows that as the alkyl chain length increases, the relative mobility of the cations decreases, which could be related to the ionic conductivity behavior with alkyl chain length. The relative mobility of the cations decreases for [BMIM][BF_4], [HMIM][BF_4], and [OMIM][BF_4] for the composition of the RTILs; however, it increases for [EMIM][BF_4], which shows the combined behavior of the viscous forces and size of the solvated cations (Eq.

27). The viscosity of the [EMIM][BF_4] was the lowest for the [BMIM][BF_4], [HMIM][BF_4], and [OMIM][BF_4], therefore it supported the increasing mobility of the cation, i.e. $[EMIM]^+$. The ionic conductivity of the RTIL system is also compared to ξ_r and shown in Figure S3 (supporting information). It could be observed from Figure S3(a) (supporting information) that with the increase of the relative ion dissociation value, ionic conductivity increases, and it reaches the maximum value at the maximum ion dissociation, then ξ_r further decreases due to the viscous forces and size of the solvated ions, which hinders the mobility of the ion, it reaches the minimum for neat RTILs where viscosity and size of the ions were maximum. In addition, Lee and Lin[18] studied ion dissociation phenomena computationally in various IL/water systems, including [EMIM][$ETSO_4$], finding a minimum dissociation where free ion activity is dominated by solvent-induced dielectric polarization. The ion dissociation minimum changes with IL concentration. The dissociated ions are solvated mainly through the solvent in the dilute region. In contrast, the ion pair stabilizes the free ions in the high concentration limit.

The ionic conductivity and ion dissociation behavior of the next RTIL system consisting of [BPM][BF_4], [B3MPY][BF_4], and [4MBBP][BF_4] in EG is shown in Figure 5. It could be observed that it follows a similar trend to imidazolium cation-based $[BF_4]^-$ anion RTILs of increasing ionic conductivity, reaching a maximum before falling as the ionic liquid concentration increases. It could also be observed that $[BPM]^+$ has lower alky chain length than $[B3MPY]^+$, and $[4MBBP]^+$ cation, and [BPM][BF_4] showed maximum ionic conductivity than [B3MPY][BF_4], and [4MBBP][BF_4]. However, the maximum conductivity value was obtained at almost the same composition of RTILs. For [BPM][BF_4], and [4MBBP][BF_4], σ_{max} showed at $x_{IL,max}$=0.5, whereas, for [B3MPY][BF_4] it showed at $x_{IL,max}$=0.4. It could be due to the viscous forces since [B3MPY][BF_4] has the lowest viscosity among pyridinium-based $[BF_4]^-$ anion RTILs, shown in Figure S1(b) (supporting information). Since [BPM][BF_4] has a higher viscosity than [B3MPY][BF_4], it could be observed from Figure S2(b) (supporting information) that both RTIL system has almost similar relative mobility of the cation. In addition, it could be observed from Figure S3(b) (supporting information) that the relative ion dissociation was maximum for [BPM][BF_4] than [B3MPY][BF_4], and [4MBBP][BF_4] in EG. Therefore, the competitive behavior of the viscous forces and size of the ions verifies the maximum ionic conductivity of [BPM][BF_4] among pyridinium-based $[BF_4]^-$ anion RTILs. Whereas [4MBBP][BF_4] has high enough viscosity to show minimum mobility of the cations resulting in the minimum ionic conductivity.

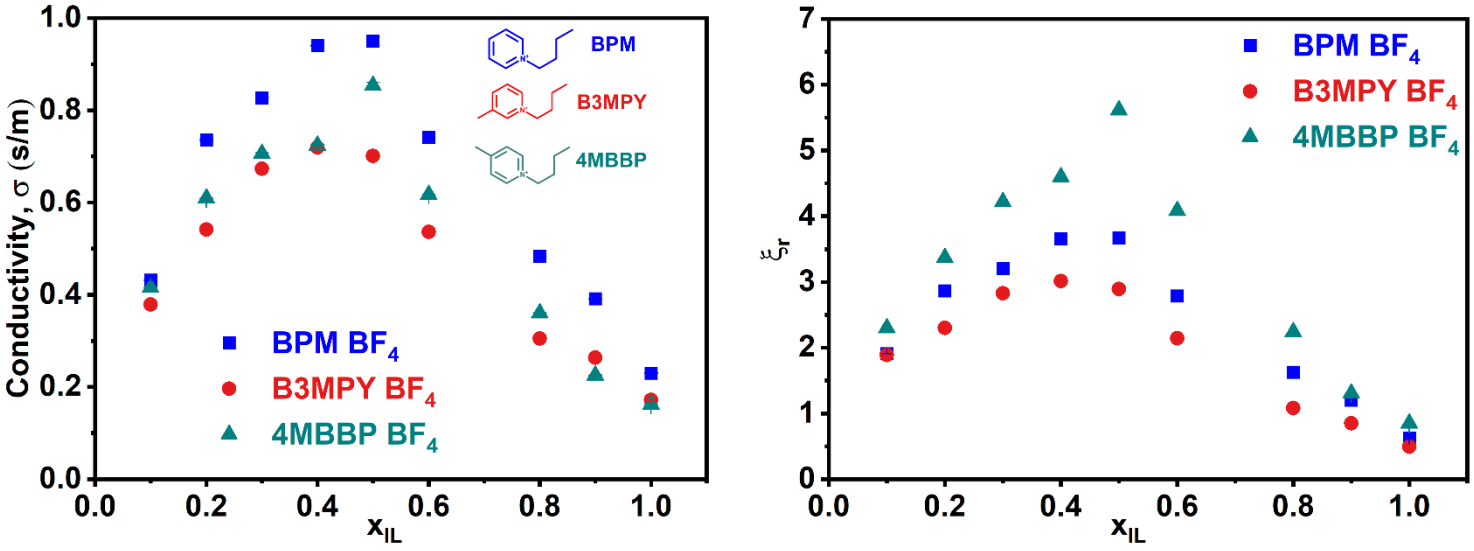

Fig. 5. (a) Ionic conductivity of [BPM][BF_4], [B3MPY][BF_4], and [4MBBP][BF_4] RTILs in EG at different mole fraction of ionic liquid estimated by the high-throughput system at 298.15 K; (b) relative ion dissociation of [BPM][BF_4], [B3MPY][BF_4], and [4MBBP][BF_4] RTILs in EG with respect to IL mole fraction.

The next RTIL mixture has a common $[OTF]^-$ anion with imidazolium and pyrrolidinium-based cations, which are $[EMIM]^+$, $[BMIM]^+$, $[OMIM]^+$, and $[BMPYRR]^+$ cation, respectively, in EG. The ionic conductivity and ion dissociation behavior of this RTIL system is shown in Figure 6. It also has a similar trend of ionic conductivity and ion dissociation with composition to the previous RTIL system. Among imidazolium-based cations with $[OTF]^-$ anion RTIL, the lowest alkyl chain length cation representing the ultimate ionic conductivity in EG, also the as the alkyl chain length increases, the composition of the RTIL in EG decreases (Figure 4). Relative ion dissociation and ionic conductivity pattern with RTIL composition have a similar fashion resulting in the ξ_r, a significant parameter to represent the conductivity behavior pattern with composition (Figure 6(b)). Therefore, this RTIL system has the following trend of ionic conductivity, [EMIM][OTF] > [BMIM][OTF] > [OMIM][OTF]. However, the ionic conductivity of [BMPYRR][OTF] lies with a composition near to [BMIM][OTF], and the maximum conductivity showed at the similar composition of [BMIM][OTF] and [OMIM][OTF] RTIL in EG. For [EMIM][OTF], σ_{max} showed at $x_{IL,max}$=0.5, whereas, [BMIM][OTF], [OMIM][OTF], and [BMPYRR][OTF] the maxima showed at $x_{IL,max}$=0.3. This behavior also results from the competitive nature of viscous forces and the type and size of the ions in the RTIL system. Figure S1(c) and Figure S2(c) (supporting information) show the RTIL viscosity and relative mobility of cation in this RTIL system. Among imidazolium and pyrrolidinium-based $[OTF]^-$ anion RTIL system, [EMIM][OTF] has the maximum ion mobility, which could be the result of the lowest viscosity which represents that it has enough lowest viscosity, showing increasing relative mobility of cation resulting maximum conductivity. In addition, Figure S3(c) (supporting information) shows a similar relative ion dissociation behavior with the ionic conductivity with previously discussed RTIL systems.

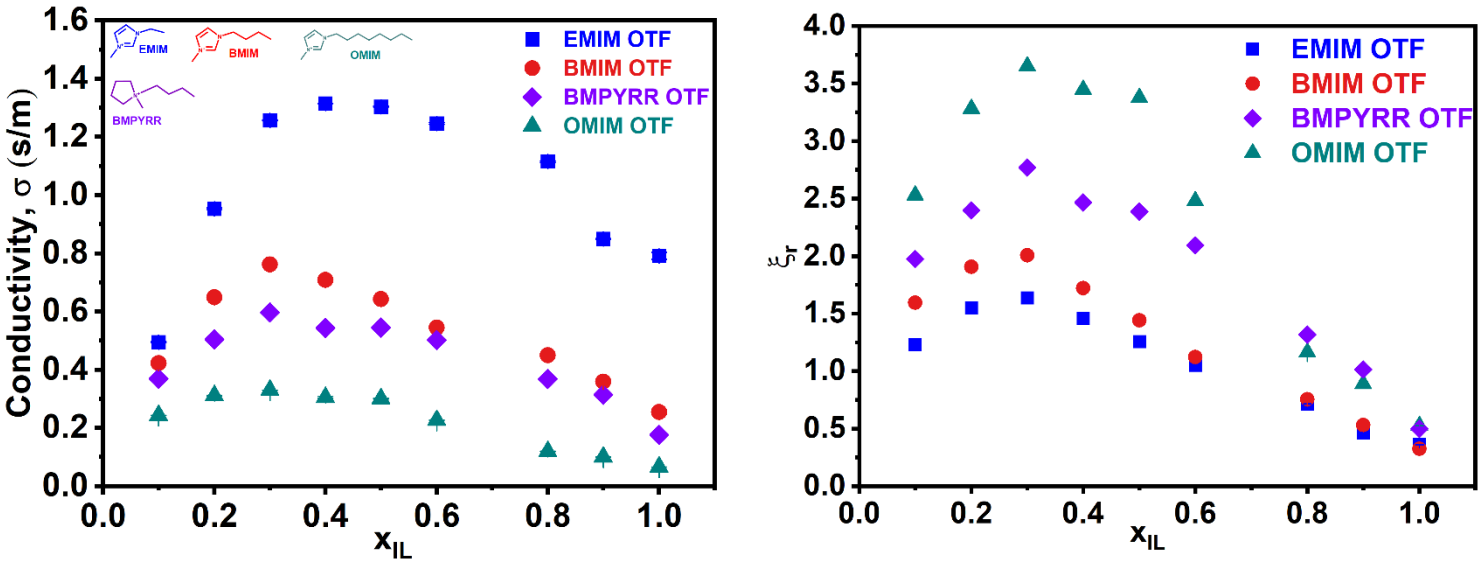

Fig. 6. (a) Ionic conductivity of [EMIM][OTF], [BMIM][OTF], [OMIM][OTF], and [BMPYRR][OTF] RTILs in EG at different mole fractions of ionic liquid estimated by the high-throughput system at 298.15 K; (b) relative ion dissociation of [EMIM][OTF], [BMIM][OTF], [OMIM][OTF], and [BMPYRR][OTF] RTILs in EG for IL mole fraction.

Similarly, the ionic conductivity and ion dissociation behavior of common iodide $[I]^-$ anion and imidazolium-based RTIL with composition is shown in Figure 7. It also has a similar trend of ionic conductivity and ion dissociation with composition with the previous RTIL system in which ionic conductivity increases with the increase of alkyl chain length. This group has an ionic conductivity trend in the following manner, [MPI][I] > [BMIM][I] > [HMIM][I]. Relative ion dissociation similarly represents the conductivity behavior pattern with composition, making it a significant parameter to define the ionic conductivity dependency with the composition of the RTILs (Figure 7(b)). However, this RTIL system showed almost similar composition for representing maximum ionic conductivity (Figure 4). Figure S1(d) and Figure S2(d) (supporting information) represent the solution viscosity and relative mobility of cation with the composition of RTIL. It could be observed that the viscosity of [MPI][I] is higher than [BMIM][I] and [HMIM][I]. Whereas the relative mobility of cation has almost the same for [MPI][I], [BMIM][I], and [HMIM][I] RTIL system, which was calculated from Eq. (27). In addition, Figure S3(d) (supporting information) represents the behavior of ionic conductivity of RTIL and ξ_r, and this represents that relative ion dissociation follows the trend of the increasing conductivity then reaching to maximum and then decreasing to the minimum. Therefore, these phenomena explain the conductivity behavior of this RTIL system in EG.

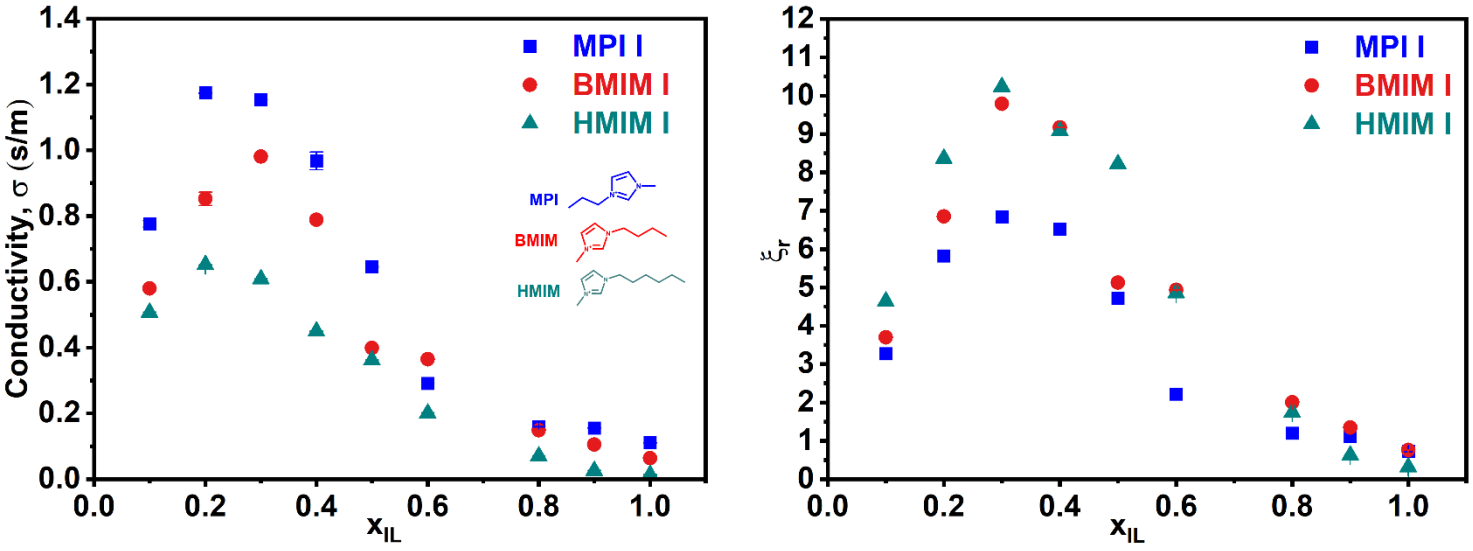

Fig. 7. (a) Ionic conductivity of [MPI][I], [BMIM][I], and [HMIM][I] RTILs in EG at different mole fractions of ionic liquid estimated by the high-throughput system at 298.15 K; (b) relative ion dissociation of [MPI][I], [BMIM][I], and [HMIM][I] RTILs in EG for IL mole fraction.

The ionic conductivity and relative ion dissociation of RTIL consisting of dicyanamide $[DCA]^-$ anion with $[EMIM]^+$ and $[BMPYRR]^+$ cation in EG was also estimated and shown in Figure 8. It could be observed from Figure 8(a) that [EMIM][DCA] has a higher concentration profile with the composition of RTIL than [BMPYRR][DCA], and it follows a similar trend with the components discussed above. [EMIM][DCA] and [BMPYRR][DCA] has σ_{max} of 3.442 s/m and 1.423 s/m at $x_{IL,max}$=0.6, and 0.4, respectively (Figure 4). It could be noted that [EMIM][DCA] shows the maximum conductivity at $x_{IL,max}$=0.6 among all the RTILs systems in EG used in this study. Figure 8(b) shows that ξ_r with composition has the trend of reaching maxima and then decreasing with composition; however, the composition position for ionic conductivity and relative ion dissociation is not similar compared to previous RTILs. The reason could be the effect of viscous forces and the structure of the cation and anion. For all the RTIL used in this study, [EMIM][DCA] has the lowest viscosity of 0.0146 Pa.s. It has the lowest viscosity profile with composition compared to all RTIL profiles of viscosity (Figure S1 (supporting information)). In addition, it also has the highest mobility profile of the cation shown in Figure S2(e) (supporting information). Therefore, it could be said that [EMIM][DCA] and [EMIM][DCA] has as the conflict behavior of the ξ_r profile to be compared with the ionic conductivity profile with composition, which could be the result of the competitive behavior of the viscous forces, structure of the anion and cation, and property of the EG. However, the ξ_r profile follows the trend of getting maxima for both the RTIL, as well as the ionic conductivity profile for ξ_r follows a similar behavior to other RTILs (Figure S3(e) (supporting information)).

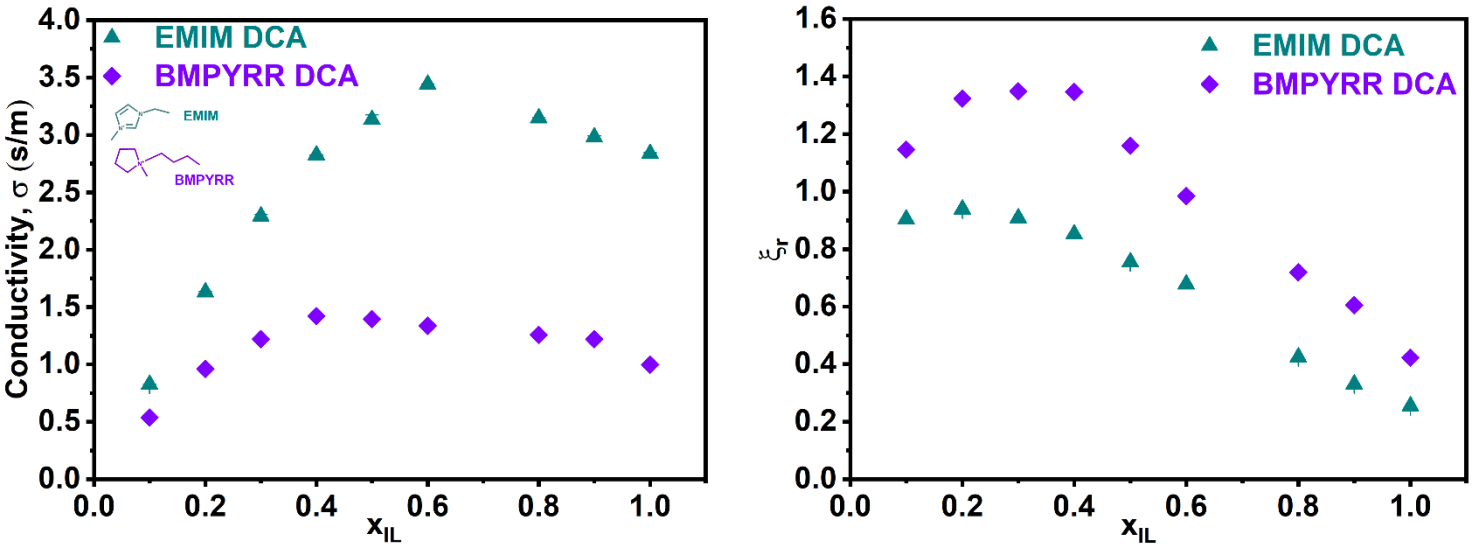

Fig. 8. (a) Ionic conductivity of [EMIM][DCA], and [BMPYRR][DCA] RTILs in EG at different mole fractions of ionic liquid estimated by the high-throughput system at 298.15 K; (b) relative ion dissociation of [EMIM][DCA], and [BMPYRR][DCA] RTILs in EG for IL mole fraction.

Similarly, another RTIL system was also used to study the ionic conductivity behavior in EG. These RTIL systems are [EMIM][SCN], [EAN], [MMIM][DMP], [EMIM][DEP] [EMIM][ESO_4], and [EMIM][HSO_4], and the ionic conductivity and relative ion dissociation are shown in Figure 9. These RTILs have different groups of cations and anions; therefore, comparing these RTILs with each other regarding ionic conductivity and relative ion dissociation is impossible. However, all have the trend of increasing ionic conductivity and relative ion dissociation with composition, reaching a maximum and decreasing to its neat RTIL value. In addition, the viscosity and relative mobility of cation with a composition are also shown in Figure S1(f-h) and Figure S2(f-h) (supporting information) for this RTIL system for understanding the competitive behavior of viscous forces and mobility of free cation. The conductivity profile for ξ_r also supports the ionic conductivity behavior in EG for these RTIL systems (Figure S3(f-h) (supporting information)).

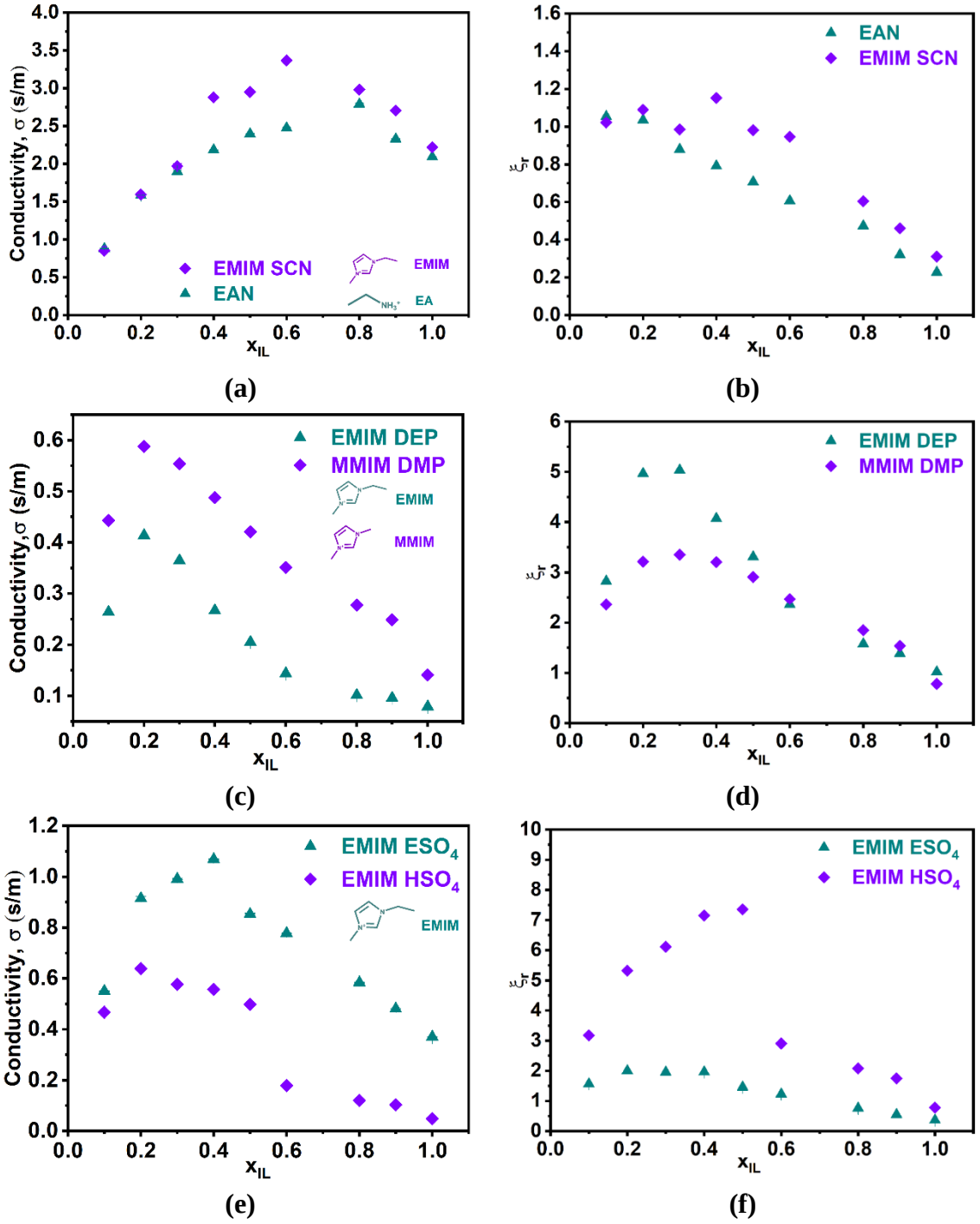

Fig. 9. (a) Ionic conductivity of [EMIM][SCN], and [EAN] RTILs in EG at different mole fractions of ionic liquid estimated by the high-throughput system at 298.15 K; (b) relative ion dissociation of [EMIM][SCN], and [EAN] RTILs in EG for IL mole fraction; (c) Ionic conductivity of [MMIM][DMP], and [EMIM][DEP] RTILs in EG at different mole fraction of ionic liquid estimated by the high-throughput system at 298.15 K; (d) relative ion dissociation of [MMIM][DMP], and [EMIM][DEP] RTILs in EG for IL mole fraction; (e) Ionic conductivity of [EMIM][ESO_4], and [EMIM][HSO_4] RTILs in EG at different mole fraction of ionic liquid estimated by the high-throughput system at 298.15 K; (f) relative ion dissociation of [EMIM][ESO_4], and [EMIM][HSO_4] RTILs in EG for IL mole fraction.

To understand the dependence of components for the composition of RTILs and ξ_r in the expression of ξ_r (Eq. (28)) are illustrated in Figures S4 to S7 (Supporting Information). It could be noted that the expression of ξr in Eq. (28) is composed of three terms: the first term is dimensionless conductivity, the second term is dimensionless viscosity, and the third term is dimensionless radii. The dimensionless viscosity term has nondissociated properties, including the viscosity of RTIL and solvent representing the viscous forces which could be said to be a type of resistance influencing the movement of the molecules within the solution. Therefore, it has significant characteristics to influence the mobility of the free ions, resulting in ionic conductivity behavior at any composition. Figure S4 (Supporting Information) represents the dimensionless viscosity term concerning the composition of the RTILs and shows that $(\eta_0/\eta_\infty)^{xIL}$ increase with the increase of the RTIL concentration in the solution. However, when this term is observed with ξ_r, it could be observed that with the increase of $(\eta_0/\eta_\infty)^{xIL}$ value, ξ_r increases and reaches maximum then decreases, which explains the ion dissociation phenomena to represent the ionic conductivity behavior of RTIL in molecular solvent (Figure S6 (Supporting Information)). The next is the dimensionless radii term shown in Figure S5 (Supporting Information) for the mole fraction of RTILs. It shows that this term has less influence than dimensionless viscosity since it has almost similar values for every RTILs. However, when plotted with respect to ξ_r, it showed a similar pattern to get maximum value then declines, which explains the ion dissociation phenomena to represent the ionic conductivity behavior of RTIL in molecular solvent (Figure S7 (Supporting Information)).

The present methodology utilizes an automated high-throughput platform to screen the mixture of RTIL system in any molecular solvent in the manner of ionic conductivity quickly. In addition, this conductivity could be utilized to study the ion mobility comprised of ion dissociation with the help of developed expression of relative ion dissociation, which needs only measurement of ionic conductivity. However, ion mobility comprised of ion dissociation phenomena is a complex behavior of the cations, anions, free ions, and viscous forces resulting in the different behavior of the properties of the RTILs in molecular solvents like EG.

4.3. Application of RTIL mixture for MAMG process

As discussed in the previous section, the mixture of RTIL and EG could achieve maximum conductivity at a specific composition of RTILs higher than neat RTILs conductivity. For [EMIM][DCA], the conductivity enhanced from 2.843 s/m to 3.442 s/m for neat RTIL and 0.6-mole fraction of RTIL in EG, respectively. Therefore, the same mixture of [EMIM][DCA] RTIL with EG was used for the MAMG process. It could be understood from Ohm's law that voltage is inversely proportional to conductivity; therefore, enhancement in the conductivity will reduce the operating voltages resulting in the reduction of energy consumption. The same concept is applied to reduce the energy consumption in the MAMG process to capture CO_2 by using higher conductivity capture media which consist of RTIL and EG.

The CO_2 capture via MAMG proceeds with the migration of the bicarbonate ions at the migration current densities of 15mA/cm^2 in the mixtures containing RTIL and EG. The pH drop in Figure 10a shows the rate of bicarbonate ions entering the aqueous compartment and decomposing to CO_2, as discussed earlier in Section 2.2. Also, based on HCO_3^--CO_3^{2-} water equilibrium, the concentration of the aqueous CO_2 was determined, as shown in Figure 10a. Since the aqueous solution was pre-equilibrated, the solution initially contained ~7mM CO_2.

However, in the presence of an external electric field, the CO_2 concentration quickly rises from 7 mM to 33 mM, reaching its maximum solubility in water. To highlight the role of conductivity in the MAMG process, we use the metric energy consumed per mol of CO_2 (E_{CO_2}). The following expression calculated the energy consumed per mol of CO_2:

$$E_{CO_2} = \frac{\mathrm{I_m} \times V}{Flux_{CO_2\ capture} \times A} \tag{32}$$

where I_m is migration current, i.e., 60 mA, V is the voltage observed during the CO_2 capture process, and A is the electrode area, i.e., 4 cm^2. The flux of the CO_2 capture process can be calculated by using the number of moles of CO_2 captured per second per unit area. For the experiments conducted with and without RTIL+EG mixture, the flux of CO_2 capture was observed to be similar and was ~0.6 mmol/(m^2.s). A comparison between energy consumed for the MAMG process with and without IL binary mixture in Figure 10b revealed a stunning decrease in energy consumption by up to 50%. Therefore, these results confirm the propitious role of RTIL+EG mixtures in enhancing the energy efficiency of the MAMG process.

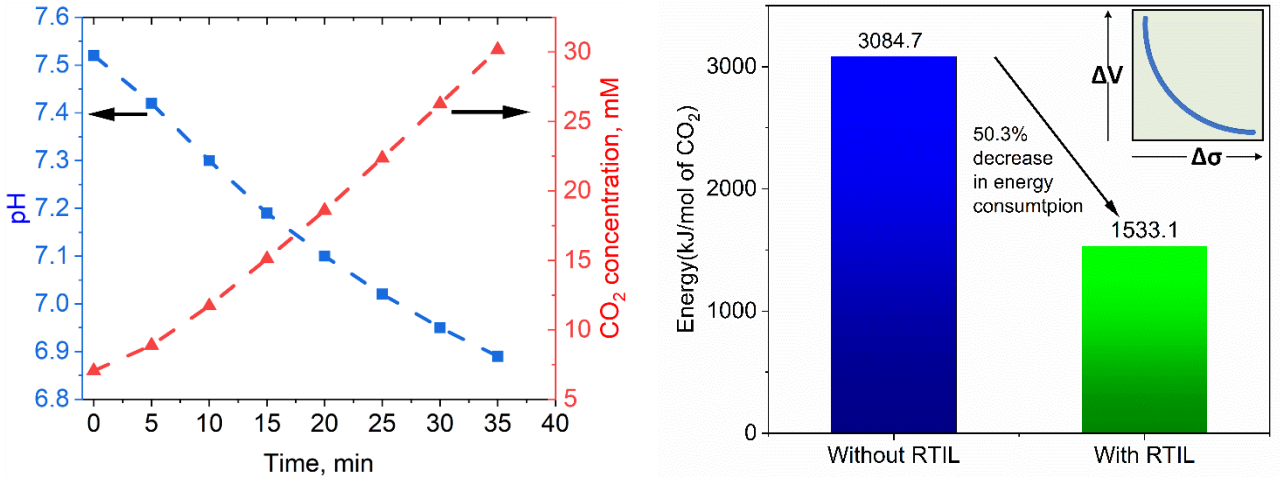

(a) **(b)**

Fig. 10. (a) Change of pH in the aqueous compartment of a MAMG process with a migration current density of 60 mA per 4 cm^2 area; (b) comparison of energy consumption to capture CO_2 with and without IL binary mixtures in a MAMG process.

5. Conclusions

This work presents a ground-breaking advancement in the high-throughput measurement and understanding of room-temperature ionic liquids (RTILs) both in their pure form and in combination with ethylene glycol (EG). By developing a comprehensive theoretical framework, we successfully elucidated the behavior of ion mobility and its impact on the ionic conductivity of RTIL-EG mixtures. Notably, our study revealed that the length of the alkyl chain in the RTILs inversely correlated with their conductivity, with [EMIM][BF4], [BPM][BF4], [EMIM][OTF], and [MPI][I] demonstrating the highest conductivity within their respective cation families. The relative ion dissociation concept provided a clear explanation for ion mobility and thus, the overall ionic conductivity across the entire concentration range, from dilute solutions to neat RTILs. This behavior can be attributed to the interplay between

free ions and viscous forces, which impact ion diffusion and ultimately affect ionic conductivity. Importantly, relative ion dissociation emerged here as a crucial parameter for characterizing ion dissociation in RTIL and molecular solvent mixtures. Our findings also identified [EMIM][DCA] as the RTIL with the highest conductivity (3.442 S/m) at a mole fraction of 0.6 within the RTIL-EG mixture. This optimized mixture offers superior conductivity and requires less energy for CO_2 absorption through the migration-assisted moisture gradient (MAMG) process compared to IL-free solutions. Additionally, we introduced a fully automated high-throughput system for efficiently measuring the conductivity, further enhancing the significance and applicability of our study. This automated high-throughput configuration represents a pioneering approach for the rapid screening of RTILs, particularly in applications where ionic conductivity plays a critical role in performance evaluation and selection.

Acknowledgments

This material is based on the work performed in the Materials and Systems Engineering Laboratory at the University of Illinois Chicago in collaboration with Dr. Jindal Shah's Lab. This material is based upon work supported by the U.S. Department of Energy, Office of Science, Office of Basic Energy Sciences Direct Air Capture program under Award Number DE-SC-0022321.

References

(1) Nordness, O.; Simoni, L. D.; Stadtherr, M. A.; Brennecke, J. F. Characterization of Aqueous 1-Ethyl-3-Methylimidazolium Ionic Liquids for Calculation of Ion Dissociation. *J Phys Chem B* **2019**, *123* (6), 1348-1358. DOI: 10.1021/acs.jpcb.8b11892 From NLM PubMed-not-MEDLINE.
(2) Nordness, O.; Brennecke, J. F. Ion Dissociation in Ionic Liquids and Ionic Liquid Solutions. *Chem Rev* **2020**, *120* (23), 12873-12902. DOI: 10.1021/acs.chemrev.0c00373 From NLM PubMed-not-MEDLINE.
(3) Liang, M.; Zhang, X. X.; Kaintz, A.; Ernsting, N. P.; Maroncelli, M. Solvation dynamics in a prototypical ionic liquid + dipolar aprotic liquid mixture: 1-butyl-3-methylimidazolium tetrafluoroborate + acetonitrile. *J Phys Chem B* **2014**, *118* (5), 1340-1352. DOI: 10.1021/jp412086t From NLM PubMed-not-MEDLINE.
(4) Humbert, M. T.; Zhang, Y.; Maginn, E. J. Assessing the reliability of computing ion pair lifetimes and self-diffusivity to predict experimental viscosity trends of ionic liquids. *Molecular Systems Design & Engineering* **2017**, *2* (3), 293-300. DOI: 10.1039/c7me00015d.
(5) Fernandes, A. M.; Rocha, M. A.; Freire, M. G.; Marrucho, I. M.; Coutinho, J. A.; Santos, L. M. Evaluation of cation-anion interaction strength in ionic liquids. *J Phys Chem B* **2011**, *115* (14), 4033-4041. DOI: 10.1021/jp201084x From NLM PubMed-not-MEDLINE.
(6) Angell, C. A.; Byrne, N.; Belieres, J. P. Parallel developments in aprotic and protic ionic liquids: physical chemistry and applications. *Acc Chem Res* **2007**, *40* (11), 1228-1236. DOI: 10.1021/ar7001842 From NLM Medline.
(7) Boruń, A. Conductance and ionic association of selected imidazolium ionic liquids in various solvents: A review. *Journal of Molecular Liquids* **2019**, *276*, 214-224.
(8) Ohligschlager, A.; Liauw, M. A. Intricate kinetics: in situ FTIR-spectroscopy discloses a phase change during ionic liquid synthesis. *Phys Chem Chem Phys* **2017**, *19* (27), 18018-18022. DOI: 10.1039/c7cp03257a From NLM PubMed-not-MEDLINE.
(9) Hall, C. A.; Le, K. A.; Rudaz, C.; Radhi, A.; Lovell, C. S.; Damion, R. A.; Budtova, T.; Ries, M. E. Macroscopic and microscopic study of 1-ethyl-3-methyl-imidazolium acetate-water mixtures. *J Phys Chem B* **2012**, *116* (42), 12810-12818. DOI: 10.1021/jp306829c From NLM Medline.
(10) Wang, H.; Wang, J.; Zhang, S.; Pei, Y.; Zhuo, K. Ionic association of the ionic liquids [C4mim][BF4], [C4mim][PF6], and [Cnmim]Br in molecular solvents. *Chemphyschem* **2009**, *10* (14), 2516-2523. DOI: 10.1002/cphc.200900438 From NLM PubMed-not-MEDLINE.
(11) Singh, T.; Kumar, A. Aggregation behavior of ionic liquids in aqueous solutions: effect of alkyl chain length, cations, and anions. *J Phys Chem B* **2007**, *111* (27), 7843-7851. DOI: 10.1021/jp0726889 From NLM PubMed-not-MEDLINE.
(12) Jarosik, A.; Krajewski, S. R.; Lewandowski, A.; Radzimski, P. Conductivity of ionic liquids in mixtures. *Journal of Molecular Liquids* **2006**, *123* (1), 43-50. DOI: 10.1016/j.molliq.2005.06.001.
(13) Tokuda, H.; Tsuzuki, S.; Susan, M. A. B. H.; Hayamizu, K.; Watanabe, M. How ionic are room-temperature ionic liquids? An indicator of the physicochemical properties. *The Journal of Physical Chemistry B* **2006**, *110* (39), 19593-19600.
(14) Zhang, L.; Xu, Z.; Wang, Y.; Li, H. Prediction of the solvation and structural properties of ionic liquids in water by two-dimensional correlation spectroscopy. *J Phys Chem B* **2008**, *112* (20), 6411-6419. DOI: 10.1021/jp8001349 From NLM PubMed-not-MEDLINE.
(15) Katayanagi, H.; Nishikawa, K.; Shimozaki, H.; Miki, K.; Westh, P.; Koga, Y. Mixing schemes in ionic liquid-H2O systems: A thermodynamic study. *Journal of Physical Chemistry B* **2004**, *108* (50), 19451-19457. DOI: 10.1021/jp0477607.

(16) Kato, H.; Nishikawa, K.; Murai, H.; Morita, T.; Koga, Y. Chemical Potentials in Aqueous Solutions of Some Ionic Liquids with the 1-Ethyl-3-methylimidazolium Cation. *Journal of Physical Chemistry B* **2008**, *112* (42), 13344-13348. DOI: 10.1021/jp806658t.
(17) Nordness, O.; Miranda, A.; Brennecke, J. F. Effects of Polarity and Hydrogen Bonding on Physical Properties and Ion Dissociation in 1-Ethyl-3-methylimidazolium Ionic Liquid plus Non-aqueous Solvent Systems. *Journal of Chemical and Engineering Data* **2021**, *66* (2), 1191-1200. DOI: 10.1021/acs.jced.0c00987.
(18) Lee, B. S.; Lin, S. T. The Origin of Ion-Pairing and Redissociation of Ionic Liquid. *J Phys Chem B* **2017**, *121* (23), 5818-5823. DOI: 10.1021/acs.jpcb.7b01189 From NLM PubMed-not-MEDLINE.
(19) Dhakal, P.; Shah, J. K. Developing machine learning models for ionic conductivity of imidazolium-based ionic liquids. *Fluid Phase Equilibria* **2021**, *549*, 113208. DOI: ARTN 113208

10.1016/j.fluid.2021.113208.
(20) Li, J. L.; He, C. C.; Peng, C. J.; Liu, H. L.; Hu, Y.; Paricaud, P. Modeling of the Thermodynamic Properties of Aqueous Ionic Liquid Solutions with an Equation of State for Square-Well Chain Fluid with Variable Range. *Industrial & Engineering Chemistry Research* **2011**, *50* (11), 7027-7040. DOI: 10.1021/ie102156m.
(21) Fuoss, R. M.; Kraus, C. A. Properties of electrolytic solutions. IV. The conductance minimum and the formation of triple ions due to the action of coulomb forces1. *Journal of the American Chemical Society* **1933**, *55* (6), 2387-2399.
(22) Justice, M.-C.; Justice, J.-C. Ionic interactions in solutions. I. The association concepts and the McMillan-Mayer theory. *Journal of Solution Chemistry* **1976**, *5*, 543-561.
(23) Krienke, H.; Barthel, J. MSA models of ion association in electrolyte solutions. *Zeitschrift Fur Physikalische Chemie-International Journal of Research in Physical Chemistry & Chemical Physics* **1998**, *204* (1-2), 71-83. DOI: DOI 10.1524/zpch.1998.204.Part_1_2.071.
(24) Valeriani, C.; Camp, P. J.; Zwanikken, J. W.; van Roij, R.; Dijkstra, M. Ion association in low-polarity solvents: comparisons between theory, simulation, and experiment. *Soft Matter* **2010**, *6* (12), 2793-2800. DOI: 10.1039/c001577f.
(25) Noda, A.; Hayamizu, K.; Watanabe, M. Pulsed-gradient spin− echo 1H and 19F NMR ionic diffusion coefficient, viscosity, and ionic conductivity of non-chloroaluminate room-temperature ionic liquids. *The Journal of Physical Chemistry B* **2001**, *105* (20), 4603-4610.
(26) Lopes, C.; Velho, P.; Macedo, E. A. Predicting the ionicity of ionic liquids in binary mixtures based on solubility data. *Fluid Phase Equilibria* **2023**, *567*, 113717.
(27) Zheng, Y.; Zheng, Y.; Wang, Q.; Wang, Z. Density, viscosity, and electrical conductivity of 1-alkyl-3-methylimidazolium dicyanamide ionic liquids. *Journal of Chemical & Engineering Data* **2020**, *66* (1), 480-493.
(28) Zhang, Q. G.; Sun, S. S.; Pitula, S.; Liu, Q. S.; Welz-Biermann, U.; Zhang, J. J. Electrical Conductivity of Solutions of Ionic Liquids with Methanol, Ethanol, Acetonitrile, and Propylene Carbonate. *Journal of Chemical and Engineering Data* **2011**, *56* (12), 4659-4664. DOI: 10.1021/je200616t.
(29) Aranowski, R.; Cichowska-Kopczyńska, I.; Dębski, B.; Jasiński, P. Conductivity and viscosity changes of imidazolium ionic liquids induced by H2O and CO2. *Journal of Molecular Liquids* **2016**, *221*, 541-546.
(30) Xu, L.; Cui, X.; Zhang, Y.; Feng, T.; Lin, R.; Li, X.; Jie, H. Measurement and correlation of electrical conductivity of ionic liquid [EMIM][DCA] in propylene carbonate and γ-butyrolactone. *Electrochimica Acta* **2015**, *174*, 900-907.

(31) Otero-Mato, J. M.; Montes-Campos, H.; Gomez-Gonzalez, V.; Montoto, M.; Cabeza, O.; Kondrat, S.; Varela, L. M. Structure, dynamics and conductivities of ionic liquid-alcohol mixtures. *Journal of Molecular Liquids* **2022**, *355*, 118955. DOI: ARTN 118955

10.1016/j.molliq.2022.118955.
(32) Stoppa, A.; Hunger, J.; Buchner, R. Conductivities of Binary Mixtures of Ionic Liquids with Polar Solvents. *Journal of Chemical and Engineering Data* **2009**, *54* (2), 472-479. DOI: 10.1021/je800468h.
(33) Ciocirlan, O.; Croitoru, O.; Iulian, O. Viscosity of binary mixtures of 1-ethyl-3-methylimidazolium tetrafluoroborate ionic liquid with four organic solvents. *Journal of Chemical Thermodynamics* **2016**, *101*, 285-292. DOI: 10.1016/j.jct.2016.06.015.
(34) Ciocirlan, O.; Croitoru, O.; Iulian, O. Densities and Viscosities for Binary Mixtures of 1-Butyl-3-Methylimidazolium Tetrafluoroborate Ionic Liquid with Molecular Solvents. *Journal of Chemical and Engineering Data* **2011**, *56* (4), 1526-1534. DOI: 10.1021/je101206u.
(35) Pal, A.; Kumar, B.; Kang, T. S. Effect of structural alteration of ionic liquid on their bulk and molecular level interactions with ethylene glycol. *Fluid Phase Equilibria* **2013**, *358*, 241-249. DOI: 10.1016/j.fluid.2013.08.029.
(36) Gutiérrez, A.; Atilhan, M.; Alcalde, R.; Trenzado, J.; Aparicio, S. Insights on the mixtures of imidazolium based ionic liquids with molecular solvents. *Journal of Molecular Liquids* **2018**, *255*, 199-207.
(37) Mayr, L. M.; Bojanic, D. Novel trends in high-throughput screening. *Current opinion in pharmacology* **2009**, *9* (5), 580-588.
(38) Gregoire, J. M.; Xiang, C.; Mitrovic, S.; Liu, X.; Marcin, M.; Cornell, E. W.; Fan, J.; Jin, J. Combined Catalysis and Optical Screening for High Throughput Discovery of Solar Fuels Catalysts. *Journal of the Electrochemical Society* **2013**, *160* (4), F337-F342. DOI: 10.1149/2.035304jes.
(39) Haber, J. A.; Cai, Y.; Jung, S.; Xiang, C.; Mitrovic, S.; Jin, J.; Bell, A. T.; Gregoire, J. M. Discovering Ce-rich oxygen evolution catalysts, from high throughput screening to water electrolysis. *Energy & Environmental Science* **2014**, *7* (2), 682-688.
(40) Haber, J. A.; Xiang, C.; Guevarra, D.; Jung, S.; Jin, J.; Gregoire, J. M. High-Throughput Mapping of the Electrochemical Properties of (Ni-Fe-Co-Ce) Ox Oxygen-Evolution Catalysts. *ChemElectroChem* **2014**, *1* (3), 524-528.
(41) Park, S. H.; Choi, C. H.; Koh, J. K.; Pak, C.; Jin, S. A.; Woo, S. I. Combinatorial high-throughput screening for highly active Pd-Ir-Ce based ternary catalysts in electrochemical oxygen reduction reaction. *ACS Comb Sci* **2013**, *15* (11), 572-579. DOI: 10.1021/co400008v From NLM Medline.
(42) Liang, S.; Kinghorn, A. B.; Voliotis, M.; Prague, J. K.; Veldhuis, J. D.; Tsaneva-Atanasova, K.; McArdle, C. A.; Li, R. H.; Cass, A. E.; Dhillo, W. S. Measuring luteinising hormone pulsatility with a robotic aptamer-enabled electrochemical reader. *Nature communications* **2019**, *10* (1), 852.
(43) Soriano, A. N.; Agapito, A. M.; Lagumbay, L. J. L. I.; Caparanga, A. R.; Li, M. H. Diffusion coefficients of aqueous ionic liquid solutions at infinite dilution determined from electrolytic conductivity measurements. *Journal of the Taiwan Institute of Chemical Engineers* **2011**, *42* (2), 258-264. DOI: 10.1016/j.jtice.2010.06.003.
(44) Wong, C. L.; Soriano, A. N.; Li, M. H. Infinite dilution diffusion coefficients of [Bmim]-based ionic liquids in water and its molar conductivities. *Journal of the Taiwan Institute of Chemical Engineers* **2009**, *40* (1), 77-83. DOI: 10.1016/j.jcice.2008.06.002.
(45) Huie, M. M.; DiLeo, R. A.; Marschilok, A. C.; Takeuchi, K. J.; Takeuchi, E. S. Ionic liquid hybrid electrolytes for lithium-ion batteries: a key role of the separator–electrolyte interface in battery electrochemistry. *ACS applied materials & interfaces* **2015**, *7* (22), 11724-11731.

(46) Ito, Y.; Nohira, T. Non-conventional electrolytes for electrochemical applications. *Electrochimica Acta* **2000**, *45* (15-16), 2611-2622. DOI: Doi 10.1016/S0013-4686(00)00341-8.
(47) Requejo, P. F.; Gomez, E.; Macedo, E. A. Partitioning of DNP-Amino Acids in New Biodegradable Choline Amino Acid/Ionic Liquid-Based Aqueous Two-Phase Systems. *Journal of Chemical and Engineering Data* **2019**, *64* (11), 4733-4740. DOI: 10.1021/acs.jced.9b00052.
(48) Newman, J.; Balsara, N. P. *Electrochemical systems*; John Wiley & Sons, 2021.
(49) Bockris, J. O. M.; Amulya, K. R. *Modern Electrochemistry: Volume 1. An introduction to an interdisciplinary area*; Springer, 1970.
(50) Treybal, R. E. *Mass-Transfer Operations*; 1955.
(51) Schotte, W. Prediction of the Molar Volume at the Normal Boiling-Point. *Chemical Engineering Journal and the Biochemical Engineering Journal* **1992**, *48* (3), 167-172. DOI: Doi 10.1016/0300-9467(92)80032-6.
(52) Marcus, Y. Thermodynamics of solvation of ions. Part 5.—Gibbs free energy of hydration at 298.15 K. *Journal of the Chemical Society, Faraday Transactions* **1991**, *87* (18), 2995-2999.
(53) Prajapati, A.; Sartape, R.; Galante, M. T.; Xie, J.; Leung, S. L.; Bessa, I.; Andrade, M. H.; Somich, R. T.; Rebouças, M. V.; Hutras, G. T. Fully-integrated electrochemical system that captures CO 2 from flue gas to produce value-added chemicals at ambient conditions. *Energy & Environmental Science* **2022**, *15* (12), 5105-5117.
(54) Prajapati, A.; Sartape, R.; Rojas, T.; Dandu, N. K.; Dhakal, P.; Thorat, A. S.; Xie, J.; Bessa, I.; Galante, M. T.; Andrade, M. H. Migration-assisted, moisture gradient process for ultrafast, continuous CO 2 capture from dilute sources at ambient conditions. *Energy & Environmental Science* **2022**, *15* (2), 680-692.
(55) Sartape, R.; Prajapati, A.; Kani, N. C.; Rojas, T.; Dandu, N. K.; Dhakal, P.; Thorat, A. S.; Xie, J.; Bessa, I.; Galante, M. T. Reply to the 'Comment on "Migration-assisted, moisture gradient process for ultrafast, continuous CO 2 capture from dilute sources at ambient conditions"'by J. Casado, Energy Environ. Sci., 2022, 10.1039/D2EE00555G. *Energy & Environmental Science* **2022**, *15* (9), 3994-3996.
(56) Wang, T.; Lackner, K. S.; Wright, A. Moisture swing sorbent for carbon dioxide capture from ambient air. *Environmental science & technology* **2011**, *45* (15), 6670-6675.
(57) Shi, X.; Xiao, H.; Azarabadi, H.; Song, J.; Wu, X.; Chen, X.; Lackner, K. S. Sorbents for the direct capture of CO2 from ambient air. *Angewandte Chemie International Edition* **2020**, *59* (18), 6984-7006.
(58) Brinkmann, F.; Dam, N. E.; Deak, E.; Durbiano, F.; Ferrara, E.; Fuko, J.; Jensen, H. D.; Mariassy, M.; Shreiner, R. H.; Spitzer, P.; et al. Primary methods for the measurement of electrolytic conductivity. *Accreditation and Quality Assurance* **2003**, *8* (7-8), 346-353. DOI: 10.1007/s00769-003-0645-5.
(59) Bandrés, I.; Montaño, D. F.; Gascón, I.; Cea, P.; Lafuente, C. Study of the conductivity behavior of pyridinium-based ionic liquids. *Electrochimica acta* **2010**, *55* (7), 2252-2257.
(60) Canongia Lopes, J. N.; Esperança, J. M.; De Ferro, A. M.; Pereiro, A. B.; Plechkova, N. V.; Rebelo, L. P.; Seddon, K. R.; Vázquez-Fernández, I. Protonic ammonium nitrate ionic liquids and their mixtures: Insights into their thermophysical behavior. *The Journal of Physical Chemistry B* **2016**, *120* (9), 2397-2406.
(61) Every, H. A.; Bishop, A. G.; MacFarlane, D. R.; Oradd, G.; Forsyth, M. Transport properties in a family of dialkylimidazolium ionic liquids. *Physical Chemistry Chemical Physics* **2004**, *6* (8), 1758-1765. DOI: 10.1039/b315813f.
(62) Harris, K. R.; Kanakubo, M. Self-Diffusion Coefficients and Related Transport Properties for a Number of Fragile Ionic Liquids. *Journal of Chemical and Engineering Data* **2016**, *61* (7), 2399-2411. DOI: 10.1021/acs.jced.6b00021.

(63) Harris, K. R.; Kanakubo, M.; Tsuchihashi, N.; Ibuki, K.; Ueno, M. Effect of pressure on the transport properties of ionic liquids: 1-alkyl-3-methylimidazolium salts. *J Phys Chem B* **2008**, *112* (32), 9830-9840. DOI: 10.1021/jp8021375 From NLM PubMed-not-MEDLINE.
(64) Kanakubo, M.; Harris, K. R.; Tsuchihashi, N.; Ibuki, K.; Ueno, M. Temperature and Pressure Dependence of the Electrical Conductivity of 1-Butyl-3-methylimidazolium Bis(trifluoromethanesulfonyl)amide. *Journal of Chemical and Engineering Data* **2015**, *60* (5), 1495-1503. DOI: 10.1021/acs.jced.5b00071.
(65) Nakamura, K.; Shikata, T. Systematic dielectric and NMR study of the ionic liquid 1-alkyl-3-methyl imidazolium. *Chemphyschem* **2010**, *11* (1), 285-294. DOI: 10.1002/cphc.200900642 From NLM PubMed-not-MEDLINE.
(66) Nazet, A.; Sokolov, S.; Sonnleitner, T.; Friesen, S.; Buchner, R. Densities, refractive indices, viscosities, and conductivities of non-imidazolium ionic liquids [Et3S][TFSI],[Et2MeS][TFSI],[BuPy][TFSI],[N8881][TFA], and [P14][DCA]. *Journal of Chemical & Engineering Data* **2017**, *62* (9), 2549-2561.
(67) Papović, S.; Vraneš, M.; Gadžurić, S. A comprehensive study of {γ-butyrolactone+ 1-methyl-3-propylimidazolium bis (trifluoromethylsulfonyl) imide} binary mixtures. *The Journal of Chemical Thermodynamics* **2015**, *91*, 360-368.
(68) Reinado, C.; Pelegrina, A.; Sanchez-Rubio, M.; Artigas, H.; Lafuente, C. Thermophysical Study of Pyridinium-Based Ionic Liquids Sharing Ions. *J Chem Eng Data* **2022**, *67* (3), 636-643. DOI: 10.1021/acs.jced.1c00925 From NLM PubMed-not-MEDLINE.
(69) Stoppa, A.; Buchner, R.; Hefter, G. How ideal are binary mixtures of room-temperature ionic liquids? *Journal of Molecular Liquids* **2010**, *153* (1), 46-51.
(70) Tomimatsu, Y.; Suetsugu, H.; Yoshimura, Y.; Shimizu, A. The solubility of cellulose in binary mixtures of ionic liquids and dimethyl sulfoxide: Influence of the anion. *Journal of Molecular Liquids* **2019**, *279*, 120-126. DOI: 10.1016/j.molliq.2019.01.093.
(71) Vila, J.; Fernandez-Castro, B.; Rilo, E.; Carrete, J.; Dominguez-Perez, M.; Rodriguez, J. R.; Garcia, M.; Varela, L. M.; Cabeza, O. Liquid-solid-liquid phase transition hysteresis loops in the ionic conductivity of ten imidazolium-based ionic liquids. *Fluid Phase Equilibria* **2012**, *320*, 1-10. DOI: 10.1016/j.fluid.2012.02.006.
(72) Vila, J.; Gines, P.; Pico, J. M.; Franjo, C.; Jimenez, E.; Varela, L. M.; Cabeza, O. Temperature dependence of the electrical conductivity in EMIM-based ionic liquids - Evidence of Vogel-Tamman-Fulcher behavior. *Fluid Phase Equilibria* **2006**, *242* (2), 141-146. DOI: 10.1016/j.fluid.2006.01.022.
(73) Wang, G. X.; Xing, Z.; Zhang, X. Y.; Liu, F. J.; Zhang, Q. G. Thermodynamic, excess Properties and Intermolecular interactions of ionic liquid 1-Ethyl-3-Methylimidazolium thiocyanate and propylene carbonate mixtures. *Journal of Solution Chemistry* **2022**, *51* (5), 594-608. DOI: 10.1007/s10953-022-01154-2.
(74) Wang, R. F.; Qi, X. J.; Liu, S. M.; He, Y. D.; Deng, Y. Q. A comparison study on the properties of 1,3-dialkylimidazolium tetrafluoroborate salts prepared by halogen-free and traditional method. *Journal of Molecular Liquids* **2016**, *221*, 339-345. DOI: 10.1016/j.molliq.2016.05.092.
(75) Widegren, J. A.; Magee, J. W. Density, viscosity, speed of sound, and electrolytic conductivity for the ionic liquid 1-hexyl-3-methylimidazolium bis(trifluoromethylsulfonyl)imide and its mixtures with water. *Journal of Chemical and Engineering Data* **2007**, *52* (6), 2331-2338. DOI: 10.1021/je700329a.
(76) Zech, O.; Stoppa, A.; Buchner, R.; Kunz, W. The conductivity of imidazolium-based ionic liquids from (248 to 468) KB variation of the anion. *Journal of Chemical & Engineering Data* **2010**, *55* (5), 1774-1778.
(77) Zhang, Q. G.; Cai, S. Y.; Zhang, W. B.; Lan, Y. L.; Zhang, X. Y. Density, viscosity, conductivity, refractive index and interaction study of binary mixtures of the ionic liquid 1-

ethyl-3-methylimidazolium acetate with methyldiethanolamine. *Journal of Molecular Liquids* **2017**, *233*, 471-478. DOI: 10.1016/j.molliq.2017.03.036.
(78) Rilo, E.; Vila, J.; Garcia, M.; Varela, L. M.; Cabeza, O. Viscosity and electrical conductivity of binary mixtures of C n MIM-BF4 with ethanol at 288 K, 298 K, 308 K, and 318 K. *Journal of Chemical & Engineering Data* **2010**, *55* (11), 5156-5163.
(79) Nishida, T.; Tashiro, Y.; Yamamoto, M. Physical and electrochemical properties of 1-alkyl-3-methylimidazolium tetrafluoroborate for electrolyte. *Journal of Fluorine Chemistry* **2003**, *120* (2), 135-141.
(80) Rilo, E.; Vila, J.; Garcia-Garabal, S.; Varela, L. M.; Cabeza, O. Electrical Conductivity of Seven Binary Systems Containing 1-Ethyl-3-methyl Imidazolium Alkyl Sulfate Ionic Liquids with Water or Ethanol at Four Temperatures. *Journal of Physical Chemistry B* **2013**, *117* (5), 1411-1418. DOI: 10.1021/jp309891j.
(81) Ueno, K.; Tokuda, H.; Watanabe, M. Ionicity in ionic liquids: correlation with ionic structure and physicochemical properties. *Phys Chem Chem Phys* **2010**, *12* (8), 1649-1658. DOI: 10.1039/b921462n From NLM Medline.
(82) Nazet, A.; Sokolov, S.; Sonnleitner, T.; Makino, T.; Kanakubo, M.; Buchner, R. Densities, Viscosities, and Conductivities of the Imidazolium Ionic Liquids [Emim][Ac], [Emim][FAP], [Bmim][BETI], [Bmim][FSI], [Hmim][TFSI], and [Omim][TFSI]. *Journal of Chemical and Engineering Data* **2015**, *60* (8), 2400-2411. DOI: 10.1021/acs.jced.5b00285.

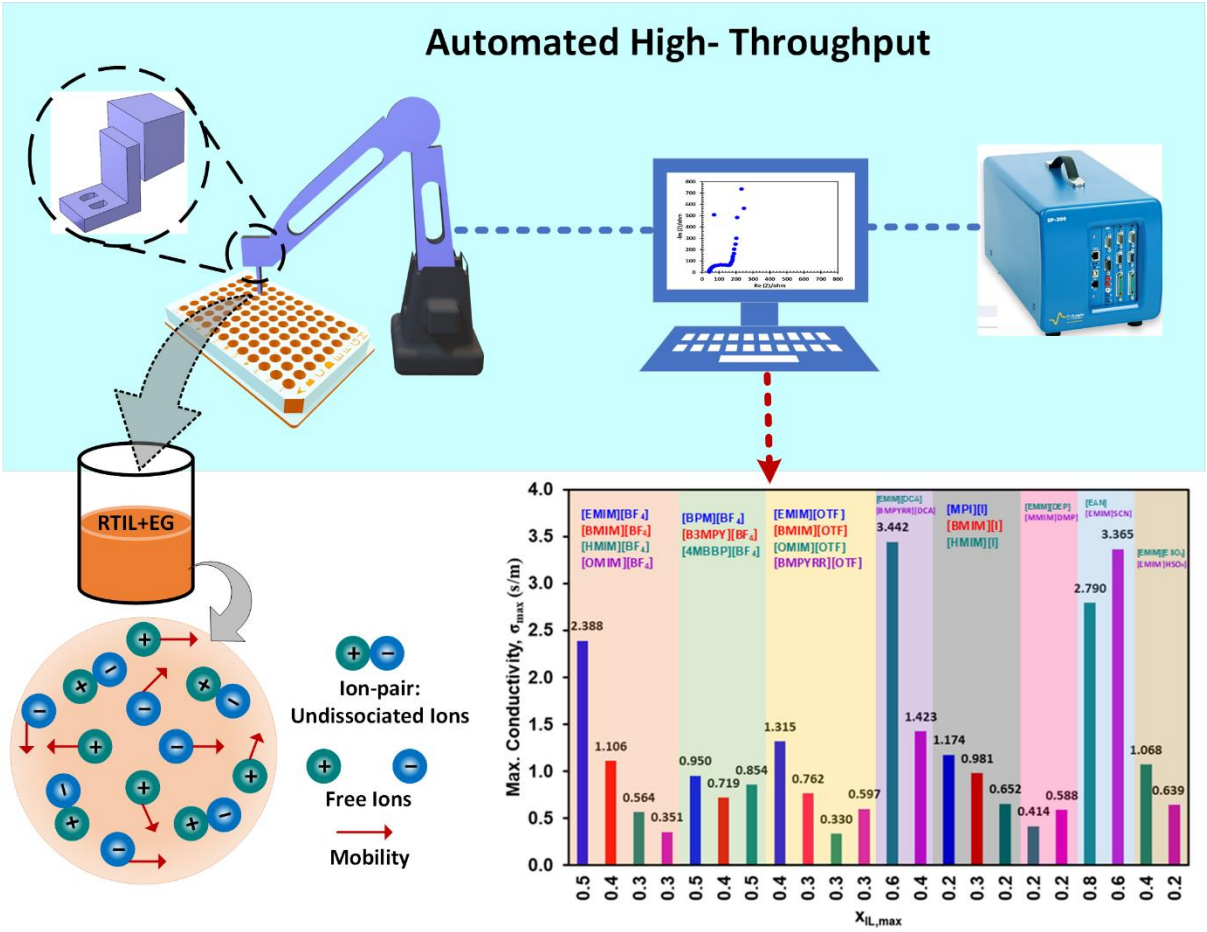

Graphical Abstract